Effect of sodium sulfate activation on the early age behaviour and microstructure development of hybrid cementitious systems containing Portland cement, and blast furnace slag.

Juan Manuel Etcheverry [1], Yury Andres Villagran-Zaccardi [1,2], Philip Van den Heede[1], Vincent Hallet [1,3], Nele De Belie[1]

[1] Magnel-Vandepitte Laboratory for Structural Engineering and Building Materials, Ghent University, Technologiepark-Zwijnaarde 60, 9052 Ghent, Belgium.

[2] Sustainable Materials, Flemish Institute for Technological Research (VITO), Boeretang 200, 2400 Mol, Belgium

[3] KU Leuven, Department of Materials Engineering, Kasteelpark Arenberg 44, 3001 Leuven, Belgium.

Abstract:

Alkali activation may help to increase the early strength and reduce the setting time of mixtures with high contents of supplementary cementitious materials (SCMs). In this research, the effect of sodium sulfate activator on reaction kinetics, compressive strength and pore structure of hybrid systems produced with 70 wt.% ground granulated blast furnace slag (GGBFS) and 30 wt.% Portland cement (PC) was determined. The setting time was shortened by adding sodium sulfate, but increasing the dose above 3 wt.% did not influence it drastically. In-situ XRD measurements revealed an increasing ettringite formation within the first 2 days of hydration. A greater reaction of the GGBFS resulted in a pore refinement of the mortars studied and consequently raised the early age compressive strength. The assessment of a convenient dosage of activator was based on both technological and environmental parameters. The contribution of PC and GGBFS to compressive strength was "decoupled".

Keywords: Hybrid binders, alkaline activator, sodium sulfate, ground granulated blast furnace slag (GGBFS), low carbon footprint.

1 Introduction

Due to the high demand and consequently vast production volumes, Portland cement (PC) production has a significant impact in the environment, not only because of the consumption of raw materials needed, but also due to the carbon dioxide emissions associated with the clinkerisation process. It is estimated that 8% of the global anthropogenic CO_2 emissions are associated with PC production [1]. Given that roughly 0.9 t of CO_2 are emitted

to produce one tonne of clinker, greener solutions can be achieved by reducing the amount of clinker in concrete mixes [2]. Ground granulated blast-furnace slag (GGBFS) derived from the iron making industry, is considered a low-carbon-dioxide by-product with an extensive track record as replacement of PC for the production of concrete. The volume of GGBFS addition allowed by existing standards is really high (up to 80% in CEM III B) [3]. However, replacing PC by GGBFS at high ratios in binder systems leads to a slow strength development particularly at early ages [4].

The use of hybrid systems comes up as an intermediate alternative to be implemented in the short term for achieving greener concretes. In such systems an alkaline activator fosters the dissolution of the SCMs but without fully replacing PC, which mainly contributes to the early age microstructure development.

Most of the studies are focused on fly ash(FA)-based hybrid systems in search of alternatives to increase the usual limited amounts that can be included in conventional PC-FA blended cements (between 30 to 35 wt%, mainly depending of the quality of the FA). Several kinds of activators were tried, but also various inconveniences were reported. Alahrache et al. [5] experimented with “mild” alkali solutions as sodium carbonate, potassium sodium silicate, potassium citrate and sodium oxalate, reporting both shorter setting times and improvements in compressive strength at early ages. However, the concentration of alkalis in the pore solutions lowers the compressive strength in the long term. Such inconvenience was less marked for sodium oxalate and potassium sodium silicate. A synergetic effect between PC and FA has been shown by using sodium sulfate together with calcium hydroxide as activators [6]. The early age hydration of high volume FA cements using gypsum and sodium sulfate as an activator was studied by [7]. It has been found that ettringite formation is reduced as alkalinity increased. An important contribution of the FA to the early age hydration was reported, which was also observed by isothermal calorimetry. However, this behaviour has not been observed in systems with lower replacement percentages, indicating that the availability of aluminates has an effect on the ettringite growth [8].

Even though the previous studies mainly focus on FA-PC systems, insights concerning the interaction between alkali-activator and PC are obtained. Much less interest has been shown in hybrid binders containing GGBFS because higher replacement ratios with GGBFS are possible due to its incipient hydraulicity. The use of alkaline activated GGBFS has been extensively studied during the last decades to produce clinker-free concrete, and it represents a promising and debated alternative to achieve ultra-low-carbon footprint systems [9]. Some authors pointed out that the availability of SCMs is not sufficient to fully supply the future demand of cement [10]. In

addition, some drawbacks have been reported for its application, with the main focus on operative issues like long setting times, poor early strength development and high (accelerated) carbonation rate due to the low content of carbonatable phases of these systems (when compared to PC concrete mixes) [11]–[14]. None of these problems are an issue when using sodium silicate / hydroxide as activator. Unfortunately, when PC is involved, the use of these kinds of strong alkaline activators is not recommended. According to [15], sodium silicate has a negative impact on the early strength development and a retarding effect on alite hydration. In addition, sodium sulfate was found to be superior over sodium hydroxide in hybrid binders.

Among possible activators, sodium sulfate is one of the most suitable based on its availability as industrial by-product, relatively low carbon footprint and good performance in presence of PC [16]–[18]. Previous studies have shown that early age strength improvement is possible with the incorporation of sodium sulfate in the blended systems [15], [19]. However, information on the early age properties of these systems is still limited. It is important to take into account that the sodium sulfate affects both the reaction of PC and GGBFS. It has been proven that sodium sulfate stimulates the hydration of alite which is the major phase in PC [20]. The understanding of this interaction of alite and C_3A with alkalis, sulfates and hydroxides at early ages [17], [18], [21], [22] has recently made much progress.

The alkaline activation of GGBFS with sodium sulfate as activator has received some attention during the last few years [23]–[27]. The information in terms of early age behaviour and the mechanism of activation for different types of slag is still limited [28], [29] since other activators have been confirmed as superior for the alkaline activation of slags, especially when it comes to providing suitable setting times and compressive strength at very early ages [30], [31]. In contrast to sodium sulfate activated slags, the addition of PC in hybrid binders is expected to drive the early age behaviour and setting times, making these systems less dependent of parameters such us slag fineness, chemical composition and activator dosage. So far, most studies cover separate investigations for GGBFS and PC, and only few studies on decoupling reactions in hybrid systems are available. Fu et al., [15] recently proposed that the enhancement in the dissolution and reaction of the GGBFS in the hybrid binder is due to a complex and cyclic mechanism which includes reduction of Ca^{2+} activity in the pore solution. Therefore, decoupling both effects in these systems is important to optimize the binder and activator proportions. As claimed by [32] [33], the MgO content (± 3%) of the slag has a significant impact on the reactivity and durability of alkali activated systems without PC. However, the use of GGBFS with different MgO contents is out of the scope of

this paper. The content of MgO in the GGBFS in this paper is similar to the European GGBFS previously reported by [29], [32] and [34].

The early stage properties including reaction kinetics are the main limitation for including higher volume of SCMs in concrete. Prince et al. [35] studied the fresh state properties of systems with 22% of alumino-silicates and pointed out that by adding alkali sulfates instead of anhydrite, ettringite does not precipitate and a rapid stiffening occurs. In addition, Rashad et al., [36] argue that the GGBFS fineness and the doses of activator are the main parameters influencing the workability and fresh state properties of alkali-activated GGBFS systems. Such properties are generally overlooked, and this can eventually bring limitations to the possible applications of hybrid systems containing GBBFS. As a consequence, the objective of this paper is to understand which are the main components (i.e. GGBFS, PC and/or Na_2SO_4) determining the setting and hardening process and the early microstructure development. In-situ XRD measurements aim to clarify the influence of sodium sulfate addition on the ettringite formation and the phase assemblage within the first 48 hours of hydration. The optimal dosage of sodium sulfate to incorporate in systems consisting of 70 % of the studied GGBFS and 30 % PC is suggested after analyzing early age properties. The role of various dosages of sodium sulfate on setting times, reaction kinetics and hardening of pastes is studied by isothermal calorimetry and ultrasonic pulse velocity (UPV). Mortars with comparable formulations to those of pastes where produced to monitor changes in compressive strength and pore structure as a function of the sodium sulfate dosage. The global warming potential per unit of characteristic compressive strength is used to determine a convenient sodium sulfate content from both a mechanical and environmental point of view. Selective dissolution is used to confirm that the increasing dissolution of the GGBFS with Na_2SO_4 observed by isothermal calorimetry results in a greater GGBFS reaction at early ages than for the blended system.

2 Materials and methods

2.1 Material characterization and mix design

Ground granulated blast furnace slag (GGBFS) and Portland cement (PC) were used in this study, with chemical compositions, densities and particle size distributions as listed in Table 1. The particle size distribution was determined by laser diffraction using a Malvern Mastersizer 2000 device. The dispersant medium used to

determine the particle size distribution of the CEM I and GGBFS was Propan-2-ol (technical grade with a purity >98%); d10, d50 and d90 are the percentiles in volume. The sodium sulfate (technical grade with a purity >99%) was added as dry solid into the mixes, the dosages used ranged from 0 wt.% to 15 wt.%. respective to GGBFS. Tap water was used in all mixes. Standard sand (EN 196-1) was used as fine aggregates in the manufacture of mortar with a sand-to-binder ratio 3:1.

The ratio 70/30 GGBFS/PC for pastes and mortars was decided based on the literature in view of the fact that 30% is the maximum relative content of PC considered convenient in a hybrid system [37], and in view of achieving a sufficient portlandite reserve (provided by the PC) to offer appropriate chemical resistance (especially in terms of carbonation resistance). Along this work the term "binder" refers to GGBFS + PC. The mix designs of the studied pastes and mortars are presented in Table 2, Table 3 and Table 4. The designation of the samples is as follows: P (paste) / M(mortar); the first S (slag) / Q (quartz); and the second S (sodium sulfate) followed by a number which represents its dosage in weight percentage of the GGBFS or quartz.

Table 1. Chemical composition and physical properties of PC and GGBFS.

Chemical composition [% m/m]	CEM I	GGBFS
CaO	64.30	40.80
SiO_2	18.30	33.30
MgO	1.40	7.84
Al_2O_3	5.20	12.30
Fe_2O_3	4.00	0.39
Mn_2O_3	-	0.36
Cl	0.06	-
BaO	-	0.31
SO_3	3.50	2.30
Na_2O	0.32	0.44
K_2O	0.43	0.67
TiO_2	-	2.30
Insoluble residue	0.40	-
Vitreous content	-	> 95.8
CaO + MgO + SiO_2	84.00	81.94
(CaO + MgO) / SiO_2	3.59	1.46

Physical Properties		
Particle size distribution (μm) d10 / d50 / d90	2.349 / 10.816 / 29.442	1.329 / 7.626 / 26.774
Density [Kg/m^3]	3160	2890

Table 2. Mix proportions of the studied pastes [g].

Designation	P-SS0	P-SS3	P-SS5	P-SS8	P-SS10
Na_2SO_4	0.0	10.5	17.5	28.0	35.0

* The content of PC (150 g), Water (150 g) and GGBFS (350 g) was the same for all these pastes.

Table 3. Mix proportions of the studied mortars [g].

Designation	M-SS0	M-SS3	M-SS5	M-SS8	M-SS10
Na_2SO_4	0.0	9.5	15.9	25.4	31.7

* The content of PC (136 g), Water (204 g), GGBFS (317 g) and Sand (1359 g) was the same for all the mortars.

2.2 Fresh state properties of pastes

Setting times were determined using the Vicat apparatus as detailed in (EN 196-3). The FreshCon device (University of Stuttgart) [38] was used to continuously measure the ultrasonic pulse velocity (UPV) through the normal consistency pastes. Pastes were cast and compacted in two layers, then covered with polypropylene film and the longitudinal (P) and shear (S) waves versus time curves were obtained using the SmartPick software for data acquisition and processing. Along the testing time of 23 hours, samples were kept at 20° C in a 60% relative humidity (RH) environment. The picker for the determination of the P-wave onset is based on the Akaike information criterion (AIC) [38] and adapted to ultrasonic signals by [39]. The onset time of the S-wave is determined by the transformation of the time signal into a time-frequency domain by means of a continuous wavelet transformation. The time elapsed between the water-cement contact (T_0 in Fig. 4 to 7) and the beginning of the measurements was added as input to the SmartPick software. A point was recorded every 3 minutes and each point is the average of 3 wave velocities through the same sample. Additional information of the set-up, mould dimensions, software and the P/S-wave onset time pickers can be found in [40]–[42].

For isothermal calorimetry, the constituents were previously conditioned at 20 °C to avoid temperature differences at the start of the measurements. Then, they were carefully weighed on a precision scale and mixed manually

inside the vials ensuring a proper homogenization. Two minutes after contact between the water and the binder, the vials were placed in the isothermal calorimeter (TAM Air) and the heat release was recorded for 7 days. The amount of paste was 14 g in all cases.

Table 4 summarizes the composition of the studied samples through isothermal calorimetry. In addition to pastes containing GGBFS, pastes containing pure quartz with a similar particle size distribution (d10/d50/d90 (vol-%): 3/6/12 µm) were prepared to simulate the individual reaction of the PC in the hybrid system. The quartz is able to produce a similar physical effect as the GGBFS, so the filler effect on the hydration of the PC in the system could be analysed separately from the contribution of the GGBFS reaction.

For the in-situ XRD measurements, pastes SS0 and SS8 were mixed manually for 2 minutes and placed in a sample holder. The surface of the paste was smoothed and covered by a 7.5 µm Kapton film. The equipment was set at 37 °C and diffraction patterns were recorded by a (Bruker) diffractometer (D2 phaser) equipped with a (Lynxeye) detector (Bruker) with CuKα radiation at 30 kV and 10 mA. The range 6 – 55 2theta was measured, with a step size of 0.3 s/step and a total time of 811.2 seconds (13.52 min) per scan, so each scan is an average over that time. In total for 48 h this results in 214 scans. The starting times counted from the start of mixing were 8 min for sample SS0 and 13.5 min for SS8.

Table 4 Samples studied by isothermal calorimetry

Designation	PC / Binder	GGBFS / Binder	Quartz / Binder	Na_2SO_4 / GGBFS or Quartz	Water / Binder
QS0	0.30	-	0.70	0	0.45
QS3	0.30	-	0.70	0.03	0.45
QS5	0.30	-	0.70	0.05	0.45
QS8	0.30	-	0.70	0.08	0.45
QS10	0.30	-	0.70	0.10	0.45
SS0	0.30	0.70	-	0	0.45
SS3	0.30	0.70	-	0.03	0.45
SS5	0.30	0.70	-	0.05	0.45
SS8	0.30	0.70	-	0.08	0.45
SS10	0.30	0.70	-	0.10	0.45
SS12	0.30	0.70	-	0.12	0.45

Designation	PC / Binder	GGBFS / Binder	Quartz / Binder	Na_2SO_4 / GGBFS or Quartz	Water / Binder
SS15	0.30	0.70	-	0.15	0.45
SS20	0.30	0.70	-	0.20	0.45

2.3 Selective dissolution.

Pastes (Table 1) were prepared and the hydration was stopped by solvent exchange using isopropanol [43] at 1, 2, 7 and 28 days of age. The paste was ground to powder and immersed (2 cycles) in isopropanol for 15 minutes/cycle. The paste-to-isopropanol ratio was 3:100 (g/g). The material was dried at 40 °C for 8 minutes and ground to powder again (<75 µm). Results of selective dissolution are the average of triplicate determinations for each sample. Dissolutions were performed for samples with 0% and 8% sodium sulfate (SS0 and SS8) following the procedure recommended in [44].

The powders were treated with EDTA+DEA+TEA solution for 2 hours. The solution was then carefully filtered so as not to lose undissolved material and the filter paper containing the residue was dried to constant weight. Once the residue was determined, calculations were made using the Equation (1) [45] where α_{GGBFS} is the reaction degree of the GGBFS in the hydrated paste, f is the mass fraction of GGBFS in initial dry binder, p is the mass fraction of GGBFS undissolved by EDTA+DEA+TEA solution. Rb [g/100 g of binder] is the mass of residue from the pastes under study. Rpc [g/100 g of binder] is the mass of residue from the PC pastes with 0% or 8% of sodium sulfate. h is the mass of dried hydrotalcite formed for 1 g of MgO (2.35 g for pure hydrotalcite with Mg:Al = 3:1) and Ms is the percentage of MgO in the GGBFS. Further information concerning the amount of paste, amounts and preparation of EDTA+DEA+TEA solution, temperature, and mixing procedure can be found in [44].

$$\alpha_{GGBFS} = \frac{f.p + Rpc\cdot(1-f) - Rb}{f\cdot(100p - h.Ms)} \cdot 100 \qquad \text{Eq. (1)}$$

2.4 Hardened state properties of mortars

Standard mortar prisms (40x40x160 mm^3) were cast for the determination of compressive strength (EN 1015-11). They were demolded after 24 hours and kept in a curing room at > 95 % RH and 20 °C until the testing ages of 2, 7 and 28 days.

Mercury intrusion porosimetry (MIP) was performed on Pascal 140/440 Thermo Fisher equipment. Sound samples of around 8 mm particle size were obtained from the core of prismatic mortar bars. These were pre-conditioned by solvent exchange using isopropanol, as it is recommended in [43], and kept in a vacuum chamber at <0.1 bar until testing-time.

About 2 g of sample was placed in the dilatometer for each measurement. In order to fill in interarticular space, vacuum was generated, mercury was allowed to enter and a pressure of 200 kPa was applied to carry out its pre-intrusion in the low pressure device. The dilatometer was moved to the high pressure unit where the pressure was progressively increased up to 200 MPa while the intrusion curve was recorded.

Duplicate measurements were performed for each mortar type. The presented values of total volume intruded and critical pore size are the average of the two measurements carried out. The critical pore size is defined as the maximum peak in the derivative of the mercury intrusion curve. MIP tests were performed at ages of 7 and 28 days. For the computations of the pore entry size, mercury contact angle was chosen at 142 °, the surface tension of the mercury was set at 0.48 N/m.

2.5 Carbon footprint calculations

Carbon footprint calculations for 1 m^3 of mortars with 0-10 wt.% of sodium sulfate were done in SimaPro 9.1.1.1 equipped with the Ecoinvent 3.6 database. The impact method used was CML-IA for which only the global warming potential (GWP) expressed in kg CO_2 eq was considered in this study. A twofold calculation approach as described in Chen et al. [32] was applied. On the one hand, only the impacts of a basic treatment were assigned to the GGBFS. On the other hand, also the environmental burdens from steel production were partially attributed. In the basic treatment approach, GGBFS receives a full attribution of granulation, drying, grinding and stock. In the basic treatment plus economic allocation approach not only a full attribution of granulation, drying, grinding and stock is assigned to the GGBFS, but also a partial attribution of the primary process, i.e. steel production are

accounted for. To do so, a recent economic allocation coefficient (Ce) for GGBFS (=0.84%, cf. [33]) was used. A detailed overview of the life cycle inventories (LCI) that were compiled in SimaPro (using ecoinvent data) for the mortar mixes under investigation has been included in a supplementary file (Appendix A).

The obtained GWP values for 1 m³ of mortar were also normalized to the characteristic compressive strength at various ages in order to find an optimum sodium sulfate content to be used from both a mechanical and environmental viewpoint. The characteristic compressive strengths were calculated in accordance with EN 1990.

3 Results

3.1 Isothermal calorimetry

Figures 1 (a) and 1 (b) show the calorimetric tests carried out on pastes containing 70% quartz and 30% PC. The induction, acceleration and deceleration periods can be clearly identified, and they follow a coherent trend for all mixes. The induction period develops until approximately 3 hours (QS0) to 3.5 hours (QS10). Then, the acceleration period develops with greater intensity and for a shorter duration with increasing sodium sulfate content, with the time for the maximum peak reducing from 11.3 hours (QS0) to 8.3 hours (QS10). For QS0 a second peak at 18.8 hours is observed in connection with sulfate depletion in the system. Deceleration is faster for QS0, with small differences between pastes containing sodium sulfate.

For this QS series (PC + quartz), the amount of heat released is greater with the content of sodium sulfate. As it can be noted in Figure 1 (a) the total heat released after 7 days was 15% to 23% higher with the addition of sodium sulfate (130 J/g binder for QS0, and 151-160 J/g binder for QS3-QS10). The peaks of the heat flow curves increase with the amount of activator (Figure 1 (b)). The initial slope is increased as well. The sodium sulfate tends to accelerate the hydration of clinker phases as the released calcium is depleted [15]. This explains that the heat flow shows greater peaks during the first hours for the pastes with the highest sodium sulfate contents. The heat flow of these samples that released the largest amount of heat during the first 30 hours then falls below those that showed lower initial peaks. Based on the cumulative heat release, similar hydration degrees irrespective of the sodium sulfate content may be then expected at very late ages. No significant differences are observed for QS pastes with sodium sulfate contents between 5 and 10%. Then, 5% sodium sulfate may be considered a saturation point for the acceleration of the clinker reaction when no GGBFS is present in the system.

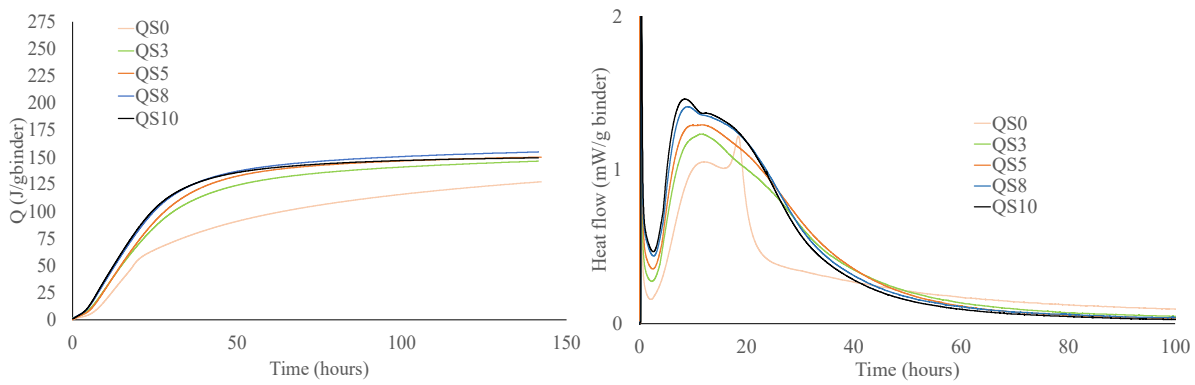

Fig. 1: Isothermal calorimetry curves for pastes with Portland cement, quartz and contents of sodium sulfate from 0% to 10%. (a) Cumulative heat released [J / g binder]. (b) Heat flow [mW / g binder].

The evolution of heat release is quite different with the incorporation of GGBFS in the system (Figure 2 (a) and (b)). The induction period is shorter with the inclusion of GGBFS instead of quartz (ranging until 2.7 hours for SS0 and until 3 hours for SS10). The differences for the end of the acceleration stage are larger for GGBFS pastes than for quartz pastes. It is noteworthy that the time for the first peak for SS0 (11 hours) is similar to the one of QS0 (11.3 hours). Overall, the cumulative heat measurements after 7 days revealed that the addition of sodium sulfate increases the hydration reaction (Figure 2 (a)), with cumulative heat release greater than in the systems without GGBFS. The similar cumulative heat release observed after 48 h for QS0 and SS0 demonstrates that the contribution of GGBFS to the formation of products that may contribute to microstructure development is very small during the first hours, and only with the inclusion of the activator it becomes meaningful. In effect, the addition of sodium sulfate affects much more the systems with GGBFS in comparison with quartz-cement pastes and it reduces the time of the first peak (to 6.7 hours for SS10). At approximately 48 h, the cumulative heat is increased by 35-45% for SS3-SS8 in comparison to SS0 and slight changes in the heat of hydration are noted when the sodium sulfate content is increased from 8% to 10%. Therefore, for the system GGBFS-PC the saturation point for sodium sulfate is rather 8% (in comparison with the 5% saturation point for the QS system). Moreover, all the samples containing sodium sulfate (SS3-SS10) show a similar behavior during the first 24 h, with only slight increases in the heat release as sodium sulfate content is increased, and in all cases with the heat release slightly higher than for the corresponding QS sample. Later, differences are accentuated depending on the amount

of sodium sulfate added. This decelerating stage is where differences to pastes with quartz are the most pronounced. For SS3 and SS5, a shoulder appears for the heat flow at around 24 h (Figure 2 (b)). For SS8 and SS10, this shoulder turns into a more significant peak that also develops with some more delay, at around 36 h. The samples with more significant heat flow during the first hours fall below the samples with less rapid reaction at around 60 h. A similar behavior is observed for the QS series (3-10%) at 30 hours. This delay in the shift between series for SS in comparison with QS can also be explained by the contribution of the GGBFS. It can be considered that the acceleration provided by the activator has completed its contribution to the microstructural development at an early age, i.e. after 60 h.

Finally, the effect of increasing doses of activator above 10% is shown in Figure 3. It is observed that as the dose is increased, the second peak becomes less pronounced and the third peak becomes more and more prolonged, moving its maximum towards later ages. The cumulative heat released after 7 days is also lower than for the sample with 10% sodium sulfate.

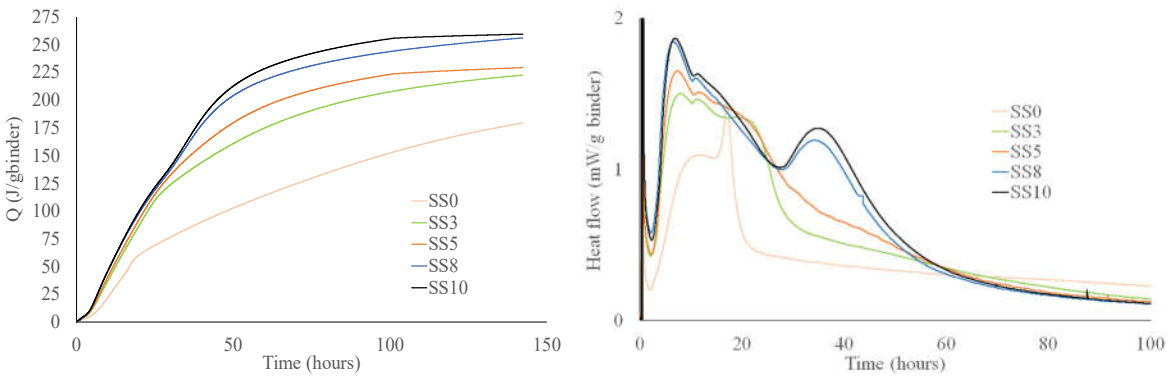

Fig. 2: Isothermal calorimetry curves for pastes with Portland cement, GGBFS and contents of sodium sulfate from 0% to 10%. (a) Cumulative heat released [J / g binder]. (b) Heat flow [mW / g binder].

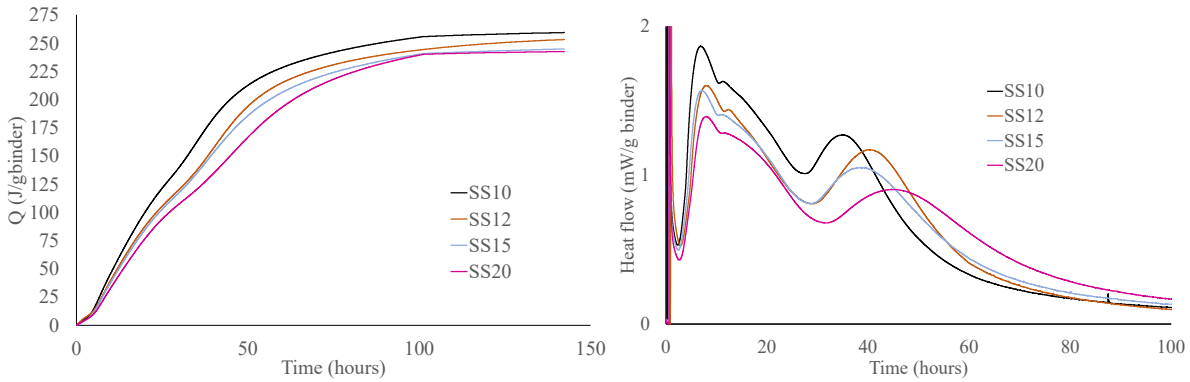

Fig. 3: Isothermal calorimetry curves for pastes with Portland cement, GGBFS and contents of sodium sulfate over 10%. (a) Cumulative heat released [J / g binder]. (b) Heat flow [mW / g binder].

3.2 Fresh state and stiffening.

The heat release measurements may be a very useful tool to monitor either the hydration process or the balance of sulfates/aluminates of "new" systems. Despite the fact many authors made correlations minute-by-minute between calorimetry and UPV, the former is not an optimum tool to correlate with the setting process, especially because either the end of the dormant period or the beginning of post-induction period are closely related to specific stages of hydration rather than the development of mechanical properties [46]. Therefore, the Vicat test was utilized in this study and complemented with the continuous recording of ultrasonic pulse velocities. Since P-waves travel through liquid, solids, and gases while S-waves travel through solid only, both types of UPV are able to complement each other. In consequence, longitudinal waves correlate with the E-modulus while shear waves are related to the G-modulus which is the one defining the stiffening process. In addition, [47] claimed that, among other properties, UPV measurements are sensitive to the effect of the ettringite and C-S-H formation.

The UPV curves for P-waves (Fig. 4) show an acceleration due to the addition of sodium sulfate. Relatively small differences are noted for the considered sodium sulfate dosing range (3-10%). In the reference sample (P-SS0), a small dormant period is noticed, followed by a rapid increase in the wave velocity. After 5 hours, an attenuation to progressively reach 2200 m/s at 23 hours is seen. With the addition of sodium sulfate, this dormant period progressively disappears, and the velocity starts to rise immediately after the filling of the moulds. An increase in the slope of the curves with the sodium sulfate content could also be noticed. Moreover, with the addition of sodium sulfate faster final velocities from 3100 m/s to 3200 m/s are observed. This slight effect of the activator

content noted for the P-waves, might suggest a trend of a faster development of a solid pathway as the sodium sulfate dosage increase. The absence of the dormant period immediately after mixing is also remarkable. Nevertheless, as many authors reported, stage I can be reduced due to several reasons others than setting [48]–[52]. It was also pointed out in [53] that early increases in the P-wave velocity are not attributed to setting while the first peak of the P-waves derivative curve is more comparable with the initial setting time.

Conversely, for S-waves in (Figure 5) the 3 stages usually reported (Figure 6) are more clear than for the P-waves. Lower transmission velocities due to the nature of the waves and their transfer medium are normal (1100 m/s for SS0 and from 1700 to 1800 m/s with sodium sulfate addition). An initial dormant period is clearly observed for all the samples, more significant than for the P-waves. With the addition of sodium sulfate, this dormant period is shorter but still visible. There seems to be, however, no differences among the various dosages of activator. This outcome is consistent with the calorimetry, as the slope of the second peak is similar irrespective of the sodium sulfate content above 3 %, and only the maximum of the peak differs (i.e. the maximum heat flow increases when the sodium sulfate content increases from 3 to 10 %, but then decreases again when the sodium sulfate content increases further from 10 to 20 %). On the other side, from 0 to 3% activator the trend is the same as for P-waves, showing an increase in the slope due to the addition of sodium sulfate. Increasing the dose of activator to more than 3% has almost no additional effect on the setting times obtained from the Vicat apparatus either (Table 5).

Some characteristic points are obtained from UPV curves and summarized in Table 5. Among them, there are the first peak of the P-waves derivative curve (dP 1st), points A (tA) and B (tB) obtained by the intersection of tangent lines as shown in Figure 6, and the point tB (P-S dif.). This point is found analogously to tB but from the curve representing the difference between P-waves and S-waves (Figure 7).

The dP 1st shifts to earlier ages as the dosage of sodium sulfate rises. Moreover, this peak occurs at an approximate velocity of 850 m/s independently of sodium sulfate content. A similar behavior is noted for tA and tB, which move to earlier times as the activator dosage increases. In P-SS0, tB occurred at a similar time as for the mixes with sodium sulfate, although the corresponding velocity is sensibly lower. tB (P-S dif.) also shows shorter times with the addition of sodium sulfate, but the differences among the several dosages are insignificant.

The initial (IST) and final (FST) Vicat setting times obtained as the average of two measurements are also included in Table 5. A significant decrease is observed with the addition of sodium sulfate, reducing the initial setting time by approximately 30% and the final setting time by approximately 35% in comparison with P-SS0. The reductions

are not only for both the initial and final setting times but also for the time elapsed between them. As mentioned above, only slight differences when increasing the dosage from 3% to 10% sodium sulfate content are noted, implying a similar effect of the sodium sulfate within this dosing range.

Initial setting times obtained by Vicat measurements are always longer than or equal to 2 hours. Similar initial setting times are obtained by the extraction of characteristic points from UPV curves which reproduces better the overall stiffening process beyond the setting time. The main outcome from the UPV analysis is that even though increasing the dosage of activator from 3 to 10% produced changes in the heat release (second peak of heat flow curves), this variation in the dosage did not significantly affect the stiffening process, which is sometimes the case when varying the dosage of alkaline activators in AAMs.

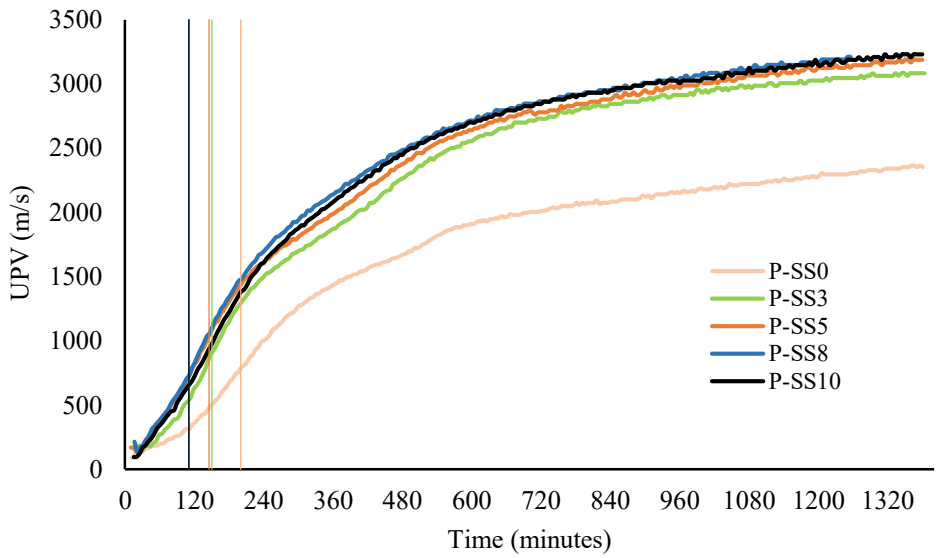

Fig. 4. Ultrasonic pulse velocity curves (longitudinal waves) for pastes with 0-10% of sodium sulfate. Vertical lines indicate the first peak of the P-waves derivative curve (dP 1st).

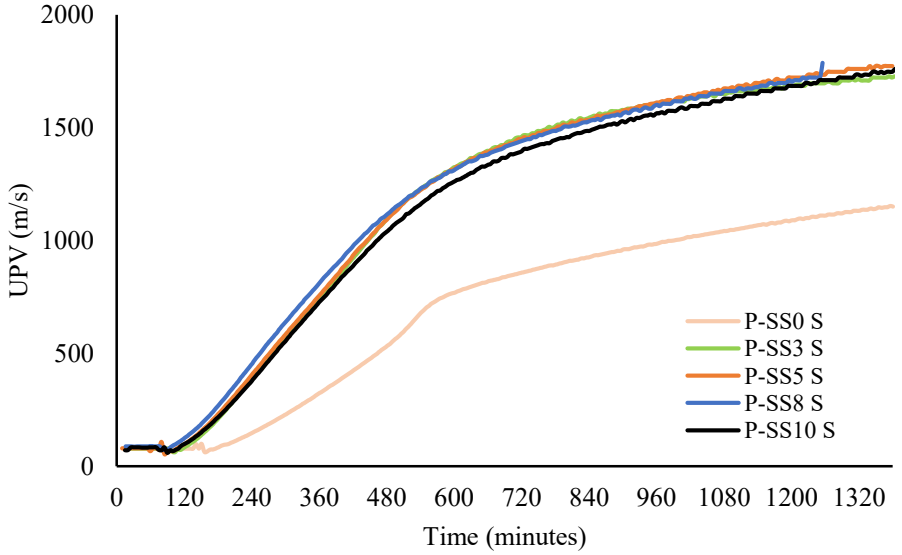

Fig. 5. Ultrasonic pulse velocity curves (shear waves) for pastes with 0-10% of sodium sulfate.

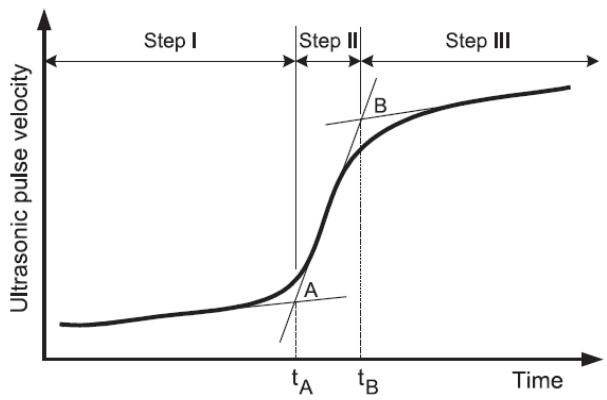

Fig. 6. Schematic representation of typical evolution of the UPV, from [54].

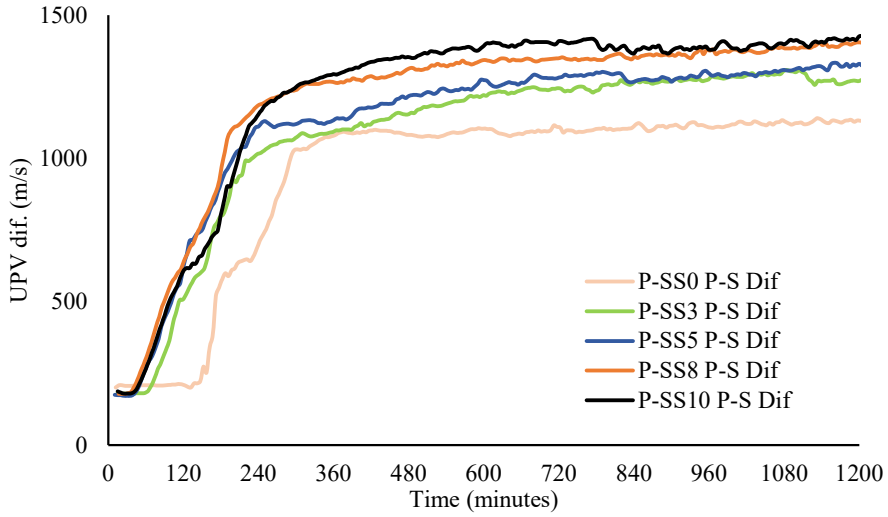

Fig. 7. Ultrasonic pulse velocity difference between P- and S-waves for pastes with 0-10% of sodium sulfate.

Table 5. Characteristic points of UPV analysis and setting times form Vicat test (minutes).

Designation	dP 1st	tA	tB	tB (P-S dif.)	IST	FST
P-SS0	200	190	580	320	180	390
P-SS3	150	140	620	270	140	280
P-SS5	145	130	600	250	130	250
P-SS8	100	120	560	260	120	270
P-SS10	100	130	580	260	120	260

3.3 In situ XRD measurements.

In-situ XRD measurements on samples SS0 and SS8 (Table 4) were carried out at 37 º C instead of 20 º C due to operative reasons. Quantifications from the XRD measurements were not possible due to a rather short duration of each scan. It is believed that increasing the temperature at which hydration is taking place would accelerate the hydration process. Therefore, in order to make minute-by-minute comparison, the reader is encouraged to check the supplementary information section on this paper where calorimetric experiments at 37 º C are included. A deeper discussion about the effect of curing temperature is out of the scope of this paper.

Results of in-situ XRD measurements are plotted in Figure 8 (SS0) and Figure 9 (SS8). A rather similar precipitation of ettringite is noted for both systems within the first 10 hours (A). Nevertheless, a reduction of the C_3S peaks intensity is observed by the addition of sodium sulfate (B). The consumption of anhydrite appears to be similar within the first 10 hours (C). Immediately after, the intensity of ettringite peaks start to rise for both mixes. However, the ettringite peaks are more intense when Na_2SO_4 is included as activator. This trend is maintained till the end of the experiment (48 hours). The consumption of anhydrite from 10 to 48 hours appears to be less marked (D) when sodium sulfate is present in the mix suggesting that even though the overall precipitation of ettringite is higher, the source it is coming from may be different after the first 10 hours (this trend might be related to the addition of the sodium sulfate as a solid powder rather than dissolved in solution).

The precipitation of CH might be more intense for SS8 within the first 15 hours (E). However, the “noise” created by the Kapton film does not allow a fair comparison, and the peaks of CH at 47 2Θ showed a similar intensity over time regardless the addition of activator.

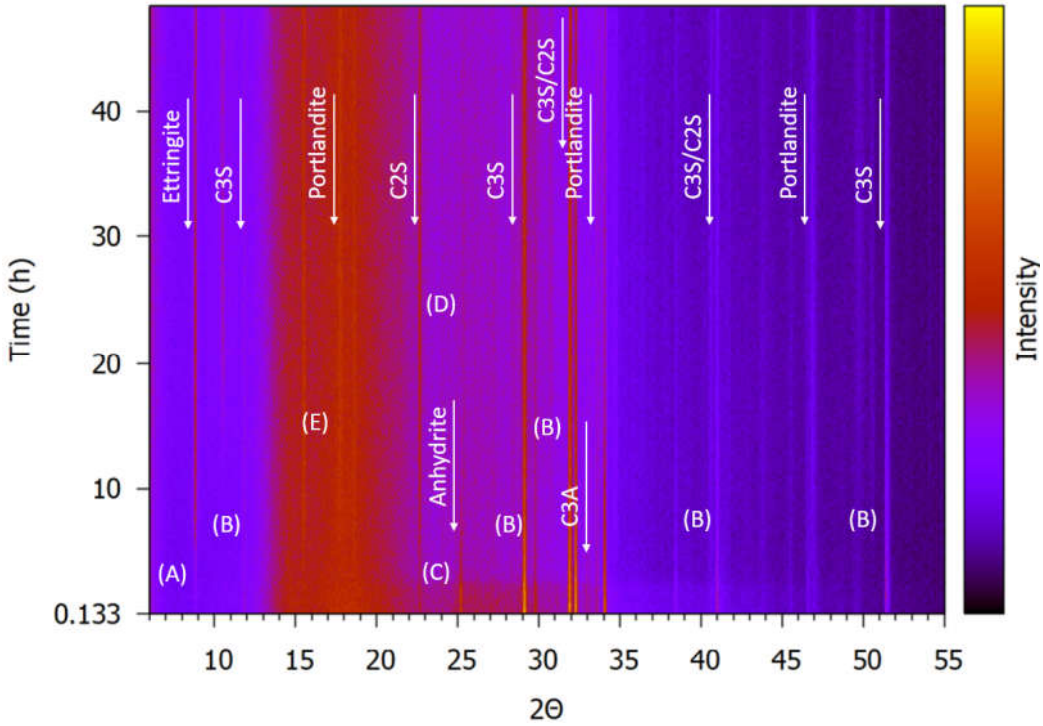

Fig. 8. In-situ XRD on SS0 samples within the first 2 days of hydration. Note: the background around 15-20 ° is normally associated with the Kapton foil.

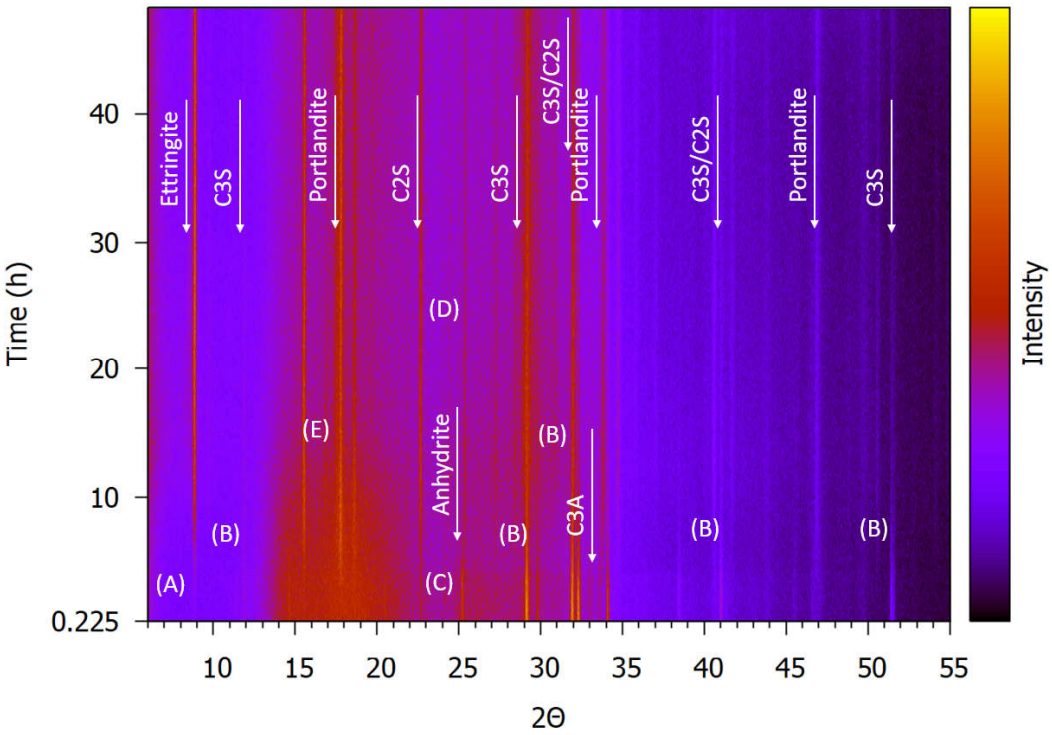

Fig. 9. In-situ XRD on SS8 samples within the first 2 days of hydration. Note: the background around 15-20 ° is normally associated with the Kapton foil.

3.4 GGBFS dissolution.

Figure 10 shows the evolution of the GGBFS reaction measured by the selective dissolution method at the ages of 1, 2, 7 and 28 days for the optimum sulfate content and the control paste without activator. Quite similar trends are observed for the two pastes, i.e. the GGBFS reacts mainly at early ages and subsequently the reaction rate starts to decrease. This is in agreement with the results of calorimetry and compressive strength. It shows that the main effects of the activator on the GGBFS and the PC reaction occurs earlier than 60 h and 48 h, respectively. However, the difference in time is less clear than in the calorimetry results as both (SS0-SS8) rise similarly between 2 and 7 days.

It is noted that after one day, the reacted GGBFS is almost 70% higher in presence of sodium sulfate. This difference is maintained until 7 days. When the evolution of the reaction rate is analyzed between 7 and 28 days, a catching up of the paste without sulfate is noticed. After 28 days, the difference in reaction degree between SS0 and SS8 becomes non-significant. The standard deviations plotted here are comparable to ones reported by [55]. The reaction degrees obtained by selective dissolution (7 and 28 days) show a very good correlation with the ones (obtained by XRD) reported by [34] in which a similar amount of sodium sulfate was added to a commercial CEM III B.

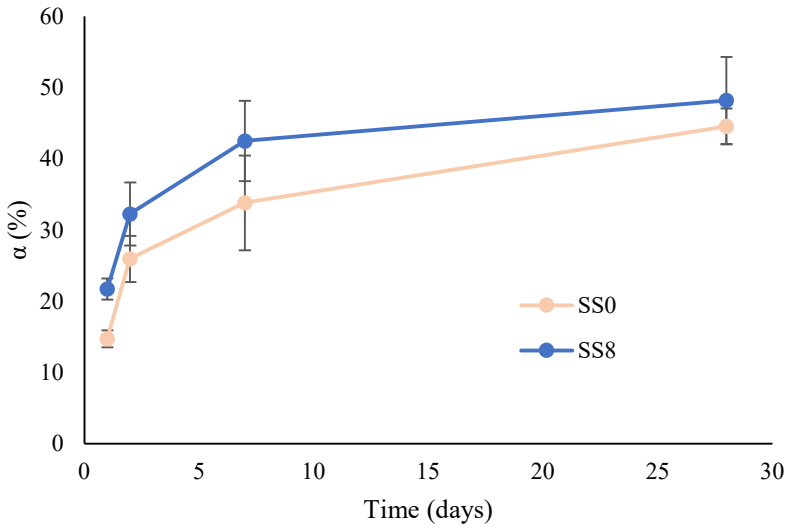

Fig. 10. Reaction degree of the GGBFS (α) in pastes with 0% and 8% of sodium sulfate at ages of 1, 2 ,7, and 28 days.

3.5 Strength gain and porosity.

Figure 11 shows the evolution of compressive strength over time for the different contents of sodium sulfate for systems containing a) Q/PC (same proportions as presented in Table 3, except that GGBFS is replaced by quartz) and b) GGBFS/PC. For systems with Q, the addition of activator results in a significant improvement in the compressive strength at very early ages, while limited differences are observed after 7 days. No further improvement is achieved by increasing the activator dosage above 3%.

For systems with GGBFS, the addition of activator results in a significant improvement in the compressive strength at all ages. By increasing the doses from 3% to 10% the compressive strength at 2 days is 1.5 to 3 times higher than the reference (M-SS0). The absolute difference in strength for the different activator contents shown at 2 days maintains at 7 and 28 days. In other words, all mixes gain similar absolute strength after 2 days. The compressive strength at 28 days is approximately 35% higher than the reference with the addition of 5%, 8% 10% and 15% sodium sulfate. However, a rise in the dosage of activator over 8% does not result in a greater strength. Then, from the point of view of strength development, 8% sodium sulfate seems to be the saturation point, in agreement with results from calorimetry.

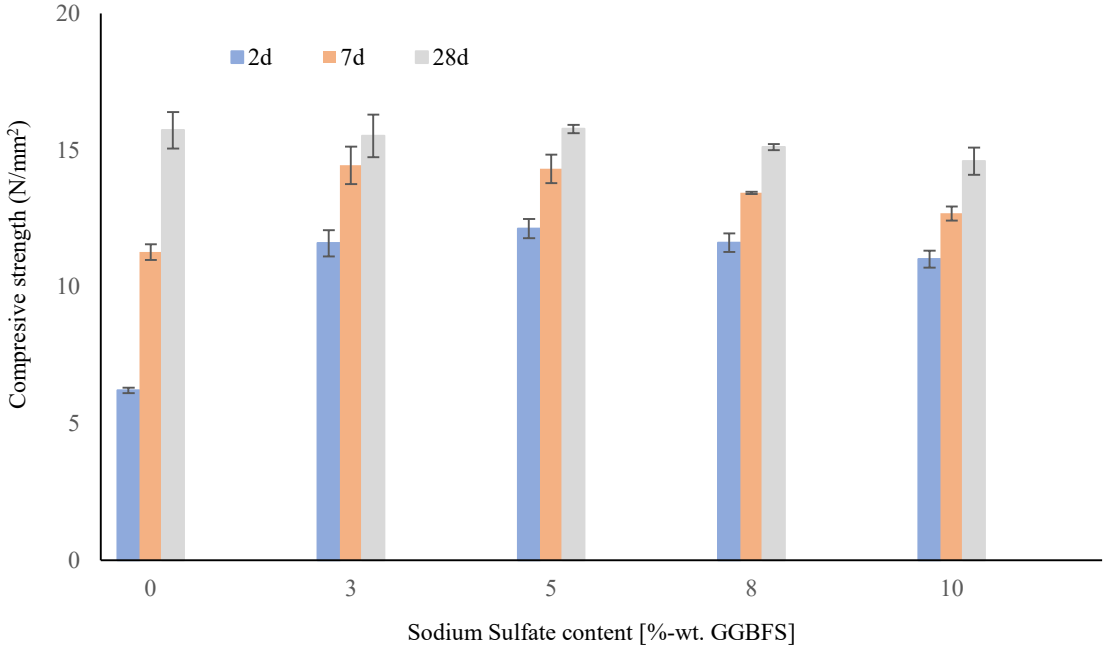

Fig. 11 a). Compressive strength in Q/PC mortars with contents of sodium sulfate from 0% to 10%.

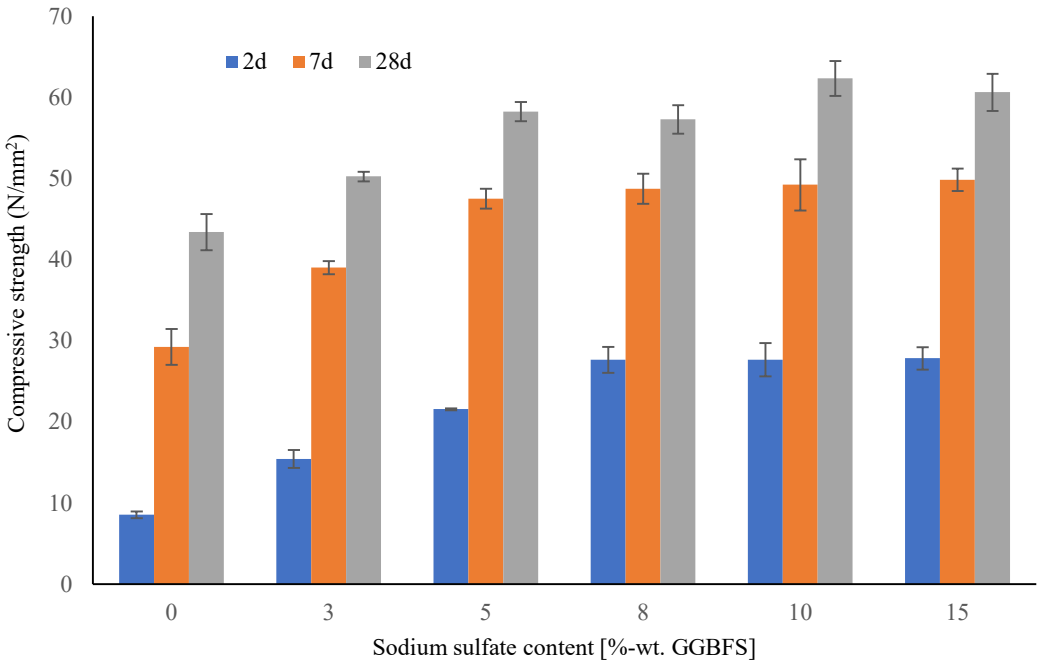

Fig. 11 b). Compressive strength in GGBFS/PC mortars with contents of sodium sulfate from 0% to 15%.

Table 6 summarizes the parameters obtained from the MIP at 7 and 28 days (Figure 12), including total intrudable volume, and critical pore sizes. The values shown are the average of 2 determinations. A reduction in the total intruded volume can be noted with the addition of sodium sulfate, regardless of the considered age.

Activator doses not only appear to influence the total amount of intrusive volume, but also the pore size distribution. Figure 12 obtained from the derivation and conversion of pressure into pore size seems to indicate reduction in mesopores (from 0.01 μm to 0.1 μm) and an increase in micropores (< 0.01 μm).

As binder hydrates a microstructure development is normally expected. From 7 to 28 days slight differences are observed without sodium sulfate (SS0), mainly in the mesopore range. However, as activator dosage increases, a larger reduction in the amount of macropores and shift to the mesopore range is noted (Figure 13).

Table 6. Pore parameters obtained by MIP at 7 days and 28 days.

Sample	Total Vol. (mm^3/g)		Critical pore size (nm)	
	7 days	28 days	7 days	28 days
SS0	52.72	47.40	15.77	7.50
SS3	51.45	46.89	13.00	9.21
SS5	44.36	43.36	33.15	21.98
SS8	44.05	40.44	33.10	32.54
SS10	37.30	36.26	24.46	24.04

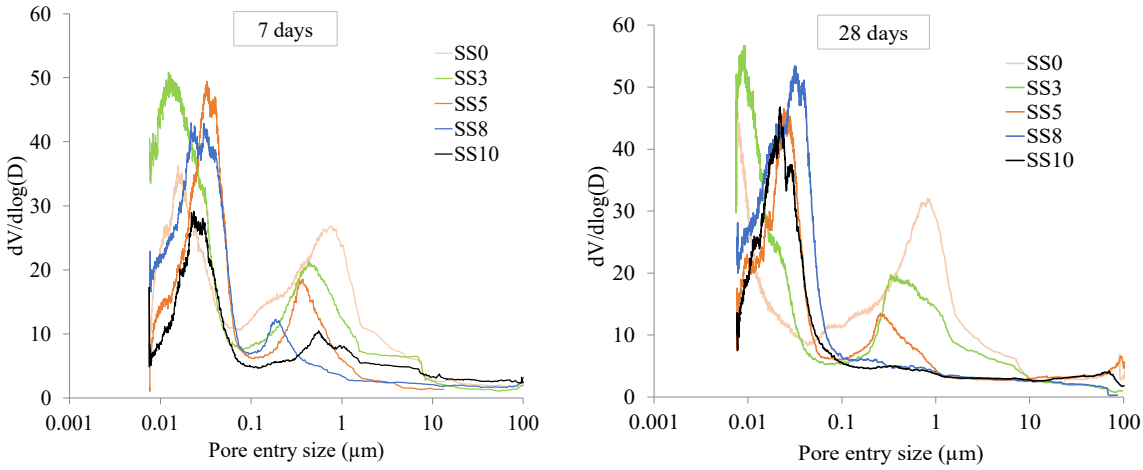

Fig. 12: Pore size distribution of mortars with sodium sulfate contents from 0% to 10% at 7 days (a) and at 28 days (b).

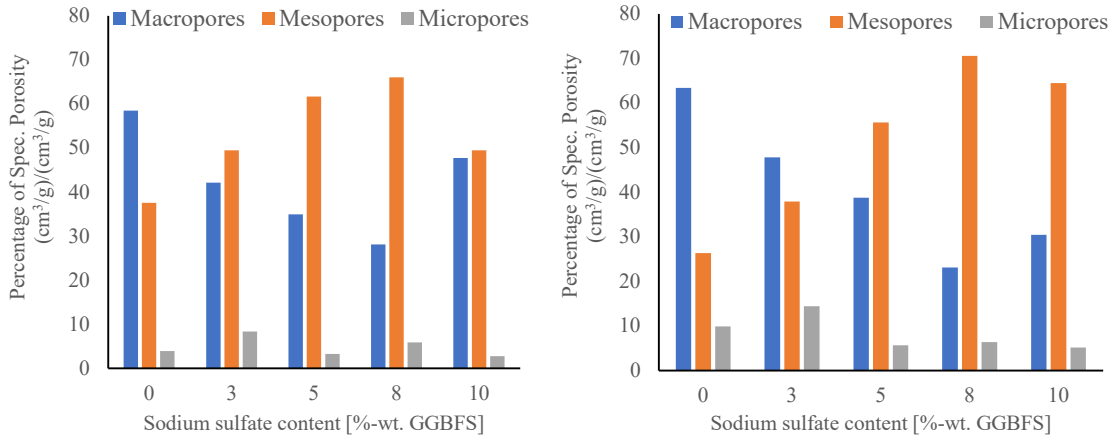

Fig. 13: Percentage of different pore fractions of mortars with sodium sulfate contents from 0% to 10% at 7 days (a) and at 28 days (b).

3.6 Carbon footprint calculations

Results of carbon footprint calculations for 1 m^3 of mortar are shown in Figure 14 (a): basic treatment for the GGBFS, and Figure 14 (a'): basic treatment plus economic allocation for the GGBFS. As expected, an increase of the impact with the added amount of sodium sulfate can be seen. Moreover, the impact of the GGBFS doubled when the economic allocation approach was considered.

When accounting for the mechanical performance of the mixtures at 2 days (Figures 14 (b-b')), at 7 days (Figures 14 (c-c')) and at 28 days (Figures 12 (d-d')), the impact in comparative terms is strongly reduced. In Figures 14

(b) and (b'), such impact is reduced by half by adding 5% to 10% sodium sulfate. When taking into consideration the compressive strength at later ages the impact of adding different dosages of sodium sulfate becomes fairly similar but slightly lower than the one without activator.

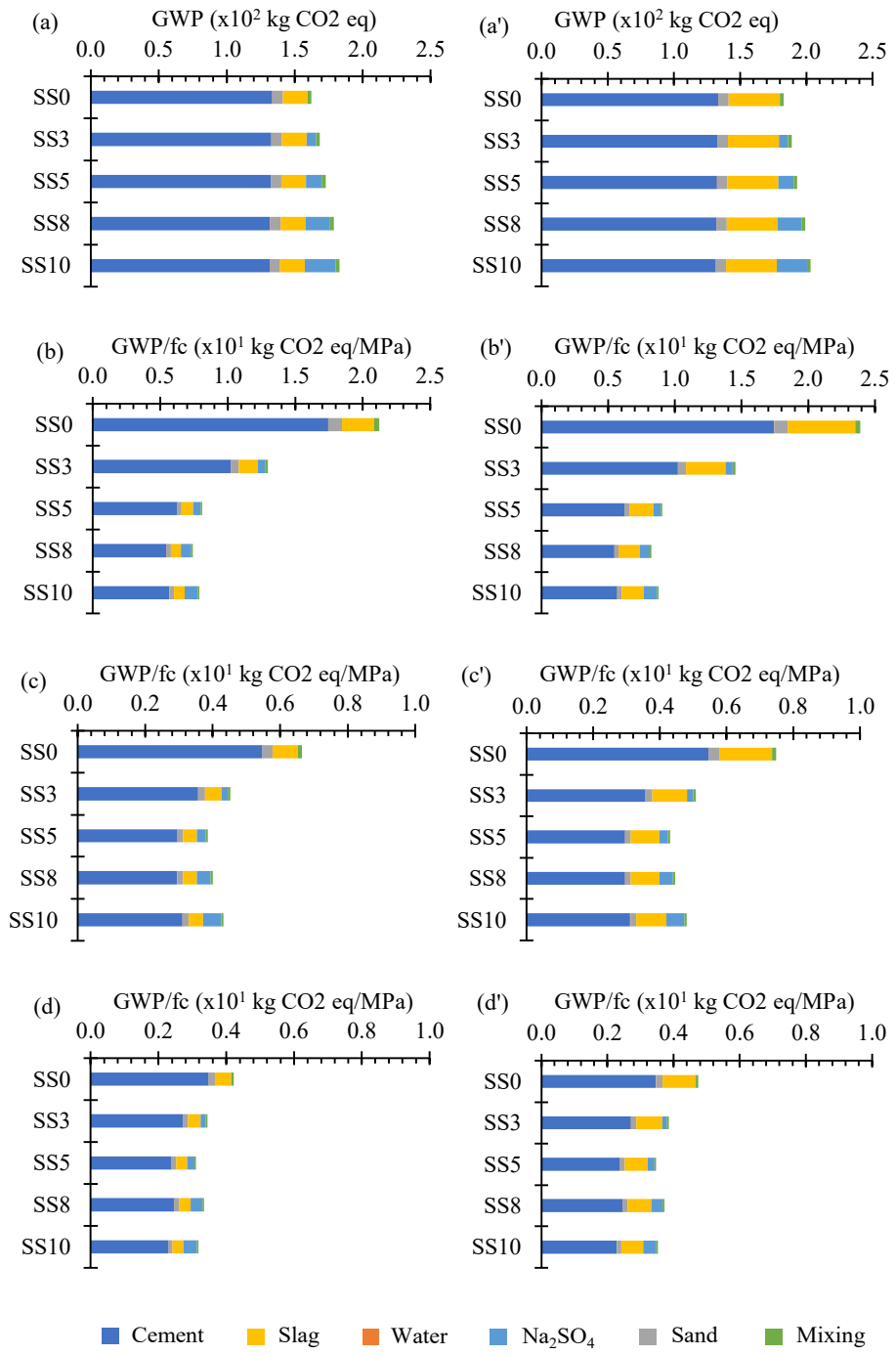

Fig. 14: (a) GWP of 1 m³ of mortar (basic treatment GGBFS (T)); **(a')** GWP of 1 m³ of mortar (basic treatment + economic allocation GGBFS (T+E)); **(b)** GWP of 1 m³ mortar per unit of 2-day characteristic compressive strength f_c (T); **(b')** GWP of 1 m³ mortar per unit of 2-day f_c (T+E); **(c)** GWP of 1 m³ mortar per unit of 7-day f_c (T); **(c')** GWP of 1 m³ mortar per unit of 7-day f_c (T+E); **(d)** GWP of 1 m³ mortar per unit of 28-day f_c (T); **(d')** GWP of 1 m³ mortar per unit of 28-day f_c (T+E).

4 Discussion

4.1 Stiffening process

In general terms, an acceleration of setting is observed due to the incorporation of sodium sulfate into the mixes. However, a rather similar effect in terms of setting and stiffening is observed regardless the increase of the dosage from 3 to 10%. Among the main factors affecting the UPV curves [47], acceleration in C-S-H formation together with the ettringite formation [56] are the ones that better explain the change in the slope at early ages when sodium sulfate is added.

Linking the stiffening process (UPV) to the hydration process (isothermal calorimetry) at very early ages was possible due to the in-situ XRD measurements.

According to the experimental data presented in section 3.1, this behaviour can be explained by the dominant role of PC in the stiffening process with the GGBFS playing a secondary role despite the increasing dose of activator. Alite is the main phase responsible for the acceleration of the hydration. The increased acceleration with Na_2SO_4 addition is mainly attributed to a faster dissolution and formation of C-S-H as reported by [18] who also argues that C-S-H needles are modified by Na_2SO_4, resulting in divergent needles structures. However, the mechanism is still uncertain.

Many authors highlight the influence of alkalis and sulfates (and the source they are coming from) on the early ettringite formation, which is also known to affect the stiffening process of cement / C_3A mixtures [35], [56]–[58]. Qualitative in-situ XRD measurements appeared to show that the earliest ettringite is in fact coming from the anhydrite rather than sodium sulfate. A similar behaviour for SS0 was observed, suggesting that the addition of sodium sulfate is not necessarily increasing the formation of ettringite within the first 10 hours. Nevertheless, sodium sulfate addition did have an influence after 10 hours (curing at 37 º C). This is in agreement with [59] who

studied the sodium sulfate addition on lime-based systems containing GGBFS and FA and concluded that a significant formation of ettringite is observed after the first 2 days of hydration.

Previous studies suggested that the alumina coming from the GGBFS may have an effect in the precipitation of ettringite as well. A recent work [60] claimed that this influence is small in terms of sulfate requirement and it does not correlate with the bulk content of alumina in the SCM. However, the presence of alkalis was reported to increase the solubility of aluminates in hybrid binders. Hence, further studies would be necessary to confirm the minor role of GGBFS (with different aluminate content) in these complex mechanisms. Quantifications coming from in-situ XRD measurements may provide valuable information in this regard.

4.2 Hydration and microstructure development

Calorimetric studies provided valuable information on the effect of the addition of sodium sulfate on the hydration progression and the development of microstructure at early age of quartz-PC and GGBFS-PC binders. On the one hand, without sodium sulfate, the reaction of the GGBFS is limited. QS0 in Figure 1 and SS0 in Figure 2 show a similar evolution of heat release during the first 24 hours. Afterwards, a little activation of the GGBFS by PC starts to be noticed. This is explained by the slow hydration capacity of the GGBFS in presence of water [61]. GGBFS reaction is activated with the release of $Ca(OH)_2$ from the cement hydration. Since the amount of PC in these systems is relatively low, the activation of the GGBFS is very slow.

Sodium sulfate accelerates the hydration and heat release of cement phases (alite in particular) [15], [17], [18]. As the dosage increases, the second peak slightly increases as well. This behaviour is observed in Figure 1 (b) and Figure 2 (b), and the similarity suggests that the accelerated dissolution of the cement phases due to the presence of sodium sulfate turns out to be independent of the presence of GGBFS. This is clearly supported by isothermal calorimetry (Figure 15) and compressive strength results in Q/PC systems, in which the speeding up of the reactions translates into a higher compressive strength at 2 days but a rather similar behaviour once the dose is increased over 3%.

When the dosage of activator is increased above 10 %, it begins to have an opposite effect on the amount of heat released , reducing not only the second peak but also the slope (Figure 3 (b)). In [15], it is suggested that the dissolution of alite occurs mainly in the first 8 hours, although, the mechanism is still uncertain. Then, it might be inferred that the increase in the content of the activator over 10 % decelerates the hydration of cement phases.

This hypothesis is in agreement with experimental data where a slight reduction in long term compressive strength of Q/PC systems was observed (Figure 11 (a)).

For the hybrid binder, the dissolution of GGBFS occurs at a later age as sodium sulfate increases above 10 %. This is also consistent with the compressive strength observed at 7 days where small differences are noted between samples M-SS5, M-SS8, M-SS10 and M-SS15. The mechanism that best explains this behaviour would be the amount of available sulfates to be adsorbed by the aluminates or by the C-S-H formed during the second peak of the calorimetry, slightly slowing down the dissolution and precipitation of the GGBFS [60]. This delay with sulfate contents above 8% to 10% appears to be in good agreement with the available amount of alumina in the GGBFS (12.3%). Considering that the Al-to-SO_4 ratio is 0.66 for ettringite and that all the alumina is forming ettringite, a maximum of (0.123 * 0.66 * 0.79) 6.5 % sulfates would be required, meaning that the excess of sulfates would remain adsorbed in C-S-H delaying the reaction or forming other phases (Fig A.4 supplementary data).

In [29], [36], studies on the activation of slag with sodium sulfate are presented. Results consistent with the ones presented here are observed, with the dissolution of the GGBFS occurring between 30 and 50 hours depending on the dosage of activator used and the GGBFS fineness. In the present study, however, by comparing the curves with quartz versus those with GGBFS, a contribution from GGBFS at earlier ages is also observed [15]. Although, as mentioned above, the cement plays a much more relevant role, not all the heat release can be attributed to cement phases only.

Figure 16, obtained as a compilation of Figure 11 (a) and Figure 11 (b) intends to decouple the contribution of PC (together with the filler effect provided by quartz) and GGBFS (in presence of PC and Na_2SO_4) to compressive strength at different ages. The results from the selective dissolution carried out on SS0 and SS8 pastes also confirm that the amount of reacted GGBFS increases significantly during the first few days due to the addition of sodium sulfate. This behavior is in line with the greater GGBFS dissolution that was observed by isothermal calorimetry. The heat contribution of the GGBFS can be calculated by measuring the total heat of SS0 (or SS8) discounted by the total heat of QS0 (or QS8) at 7 days, which when divided by the measured reaction degree by selective dissolution, gives the heat release associated to the GGBFS. These values were 221 J g^{-1} slag and 339 J g^{-1} slag for the blended and the hybrid systems. Similar calculations were presented in [34] using the regression of the slag reaction degree (measured by XRD), with suggested values of 498–510 J g^{-1} slag and 587–625 J g^{-1} slag. It

is noteworthy that these values considered the filler effect provided by the slag in the system, which have been discounted in our case. However, a similar analysis could be done at 1 and 2 days, Kocaba [62] reported discrepancies for the correlation factors (J g^{-1} slag) when comparing degree of reaction and cumulative heat at early ages.

In addition, the selective dissolution (or "preferential dissolution") values reported here should be considered with caution due to the uncertainties of the method. In this paper, the objective of determining the GGBFS "degree of reaction" was to rule out the hypothesis that the acceleration in the hydration of the cement was the only cause of the increasing compressive strength, and prove that there was a greater influence of the GGBFS in the development of microstructure by the addition of activator.

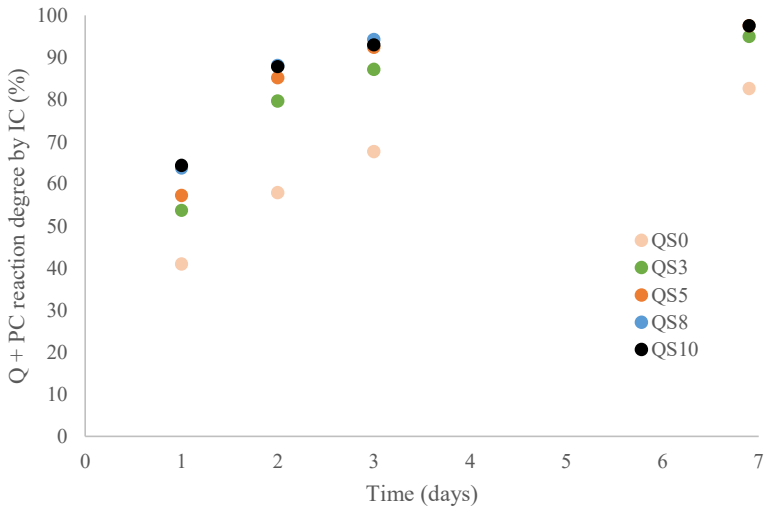

Fig. 15:. Hydration degree of PC+Q systems estimated from isothermal calorimetry.

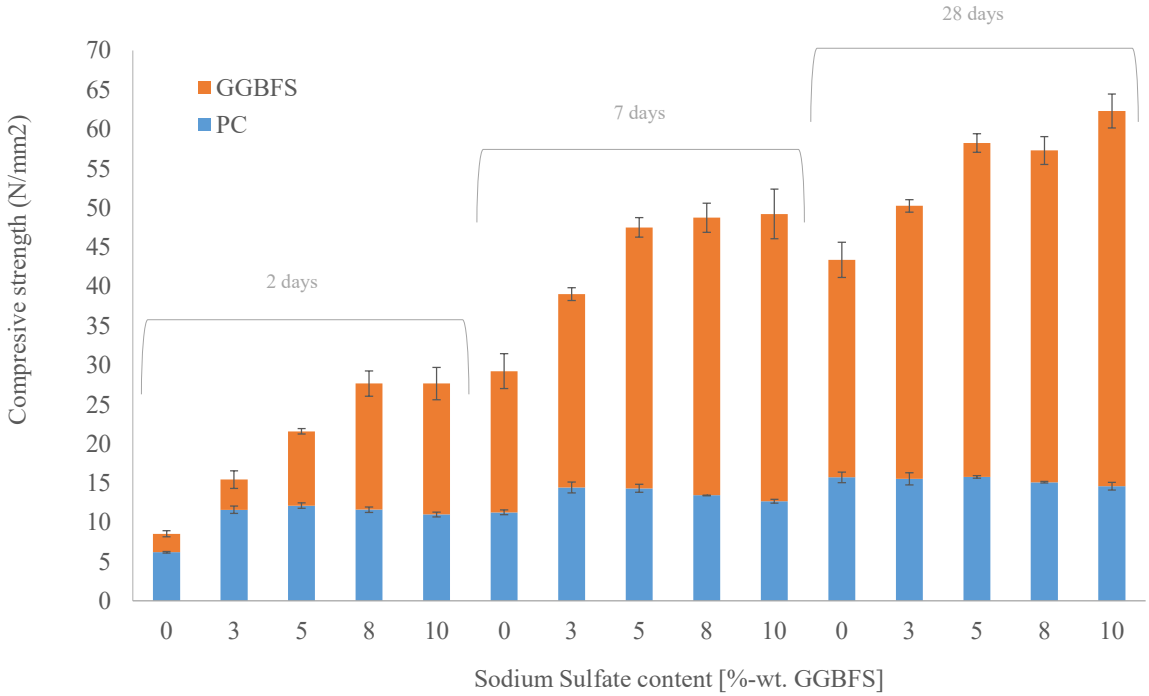

Fig. 16:. Compressive strength contribution of PC and GGBFS at 2, 7 and 28 days of hydration. Mixes containing 30% PC, 70% GGBFS and a dosage of sodium sulfate from 0 to 10%.

4.3 The pore structure

The lower volumes of intruded mercury could be preliminarily attributed to an increase in the degree of microstructure development of the whole binder (PC + GGBFS) caused by the activator (Figure 17). However, increasing dosage of activator not only appears to influence the total amount of intrusive volume, but also the pore size distribution, which seems to be due to a pore refinement action (Figure 13). Such pore refinement action was previously reported by [63] for PC-GGBFS blended cements without sodium sulfate, and attributed to an increase in tortuosity due to the high amount of GGBFS. In the present study, the amount of GGBFS is fixed but the amount of sodium sulfate varies, which triggers a greater reaction of the GGBFS within the first days of hydration, as it was observed in the third peak of the calorimetry (Figure 2 b).

Although the cement reduces voids as the microstructure develops , such pore refinement correlates better with the reaction degree of GGBFS and ettringite formation [34] than with the reaction of the whole binder system (GGBFS + PC). This can clearly be noted by comparing MIP curves for SS3 (28 days) and SS8 (7 days) in Figure 12. Both show similar compressive strengths, but the mesopores volume for SS8 is lower than the one for SS3. It

means that the increase in sodium sulfate content not only accelerates strength gain, but also seems to improve the microstructure of the hardened mortar.

The values of the critical pore size listed in Table 6 can be confusing. On the one hand, there was a reduction from 7 to 28 days for the samples containing up to 5% sodium sulfate. The lower the sodium sulfate addition was, the higher the change in the pore structure from 7 to 28 days. In addition, above 5%, the critical pore size remained similar from 7 to 28 days. This behaviour is explained by the acceleration in the GGBFS reaction caused by the activator.

On the other hand, the values of the critical pore size tended to increase with the addition of the sodium sulfate and this is mostly related to the way in which this parameter is calculated. There were initially 2 peaks and therefore the shortest peak associated to macropores is not considered by the critical pore size calculations unless 2 critical pore sizes are calculated for the same sample. Having said this, the pore refining reduced the volume of macropores so that the volume of these pores is now comparable to the ones that were considered as mesopores, increasing the mesopore volume (Figure 13). Nevertheless, this increase in the critical pore size values does not necessarily mean a negative effect on the pore structure.

The use of the (cylindrical-shaped) pore model applied in MIP to calculate the pore size distribution could also bring limitations when an important amount of needle-shaped phases like ettringite is expected in the systems [64]. Future studies will confirm or not the stability of such refining action and its possible impacts in terms of durability and transport properties will be assessed.

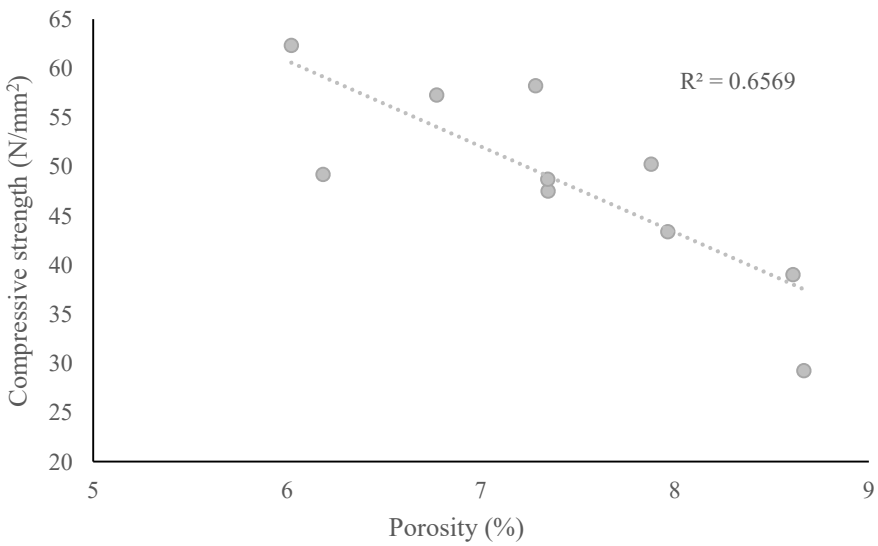

Fig. 17:. Compressive strength of M-SS0 and M-SS8 samples versus porosity (the porosity is computed from the intruded volume of mercury and the density of samples).

4.4 Environmental viewpoint

The effect of the activator is mostly shown at early ages. In the absence of sodium sulfate the GGBFS reacts more slowly; at very advanced ages the reaction degree of the GGBFS is more similar irrespective of the sodium sulfate content. Therefore, the GWP/fc tends to become similar for the systems with or without activator. The increase in GWP related to the addition of sodium sulfate seems to be low compared to the reductions in CO_2 emissions obtained by replacing PC by GGBFS also when considered per unit of compressive strength. These LCA calculations aimed to point out that the addition of sodium sulfate is more convenient than increasing the PC content of the systems. Nevertheless, in order to confirm the sustainability of these mixes, the durability of the systems has to be tested in different environmental conditions taking into consideration possible applications for this new binders.

5 Conclusions and future perspectives

The present study shows early age results of the activation of blended cements with high content of GGBFS by sodium sulfate. The main outcomes of this study are listed below:

1. There is an acceleration of setting and the overall stiffening process due to the addition of the activator. In addition, the dosage of sodium sulfate has similar influence on the setting time and stiffening for contents > 3%, as the process is mainly controlled by the effect of sodium sulfate on the cement phases.
2. A limited contribution of the GGBFS on microstructural development is observed prior to 30 hours (20 ^{o} C), where its activation occurs. The dissolution/activation of the GGBFS occurs mainly within the first 2 days since the initial water-binder contact (within the first 30 to 50 hours, depending mostly on the dosage of sodium sulfate) and subsequently all samples have a fairly similar increase in strength. In other words, early benefits of the activation of GGBFS by sodium sulfate are maintained after 48 h.
3. Increasing the sulfate content from 5 to 8% of the GGBFS showed benefits in terms of activation at early ages (< 2 days), resulting not only in improved strength but also in changes in the microstructure of the

samples where a refining action is observed. Percentages of sodium sulfate under 5 wt% of GGBFS also showed to be able to produce an improvement in early strength, but GGBFS activation is slower for such systems, especially at early ages. Low sodium sulfate contents could lead in this way to a larger accessible pore network.

4. Based on strength and early microstructure development, the use of 8% sodium sulfate with respect to the weight of the GGBFS was the optimum if a very high compressive strength is required. Above 10% sodium sulfate the effect of adding the activator ends up in impairments of the performance of the systems, delaying and reducing the GGBFS dissolution and the cumulative heat released during the first week.
5. The global warming potential is obviously influenced by the addition of sodium sulfate. However, when considering the characteristic strength of the samples, a more efficient use of the material is observed by adding sodium sulfate. Considering basic treatment and economical allocation provides a more fair approach for carbon footprint calculations since GGBFS is a by-product with a commercial value. Under these conditions, sodium sulfate dosage in the studied hybrid binder systems should not be higher than 8% from an environmental viewpoint.

In terms of future perspectives, the main research efforts still needed before moving from the laboratory to industrial application are related to the durability (e.g. sulfate attack, alkali-aggregate reaction, carbonation) and rheology (e.g. pumpability) aspects of these hybrid systems that have to be ascertained first. The resistance to internal and external sulfate attack has to be evaluated as the mechanism might not be so straight forward as in PC systems (a higher amount of sulfates does not necessarily mean more cracking when the amount of SCMs is important). In relation to the alkali-silica reaction, in principle the general rule would apply, i.e. the application of a high alkali binder is incompatible with potentially reactive aggregates. Due to the limited amount of PC in the binder, the carbonation performance (for structural applications) also deserves attention. Furthermore, little is known about the ability of concretes produced with hybrid binders to be pumped, although experimentally it was observed that the addition of the activator increases the flowability very slightly. In any case, this property appears to depend more on the concrete mix design than on the binder. In addition, the interaction with additives deserves some more attention. Finally, further research is needed to produce sufficient data to feed thermodynamic models of sodium sulfate activated hybrid binders.

CRediT authorship contribution statement

Juan Manuel Etcheverry: Conceptualization, Methodology, Formal analysis, Investigation, Writing – Original Draft, Visualization

Yury Andres Villagran-Zaccardi: Conceptualization, Methodology, Formal analysis, Investigation, Writing – Review & Editing, Supervision.

Philip Van den Heede: Formal analysis, Investigation, Writing – Review & Editing.

Vincent Hallet: Formal analysis, Investigation, Writing – Review & Editing.

Nele De Belie: Conceptualization, Resources, Writing – Review & Editing, Supervision, Project administration, Funding acquisition.

Declaration of competing interest

The authors declare that they have no known competing financial interests or personal relationships that could have appeared to influence the work reported in this paper.

Acknowledgements

The authors greatly appreciate the generosity of Prof. Susan Bernal (University of Leeds), who provided constructive feedback during the drafting of this paper. This research was funded by Research Foundation-Flanders (FWO-Vlaanderen) through research grants G062720N (JM Etcheverry and P Van den Heede) and MSCA-SoE 12ZZD21N LV (YA Villagrán-Zaccardi).

References

[1] J. G. J. Olivier, G. Janssens-Maenhout, M. Muntean, and J. Peters, “Trends in Global CO2 Emissions: 2016 Report; PBL Netherlands Environmental Assessment Agency: The Hague,” *PBL Netherlands Environ. Assess. Agency Eur. Comm. Jt. Res. Cent.*, p. 86, 2016, [Online]. Available: https://www.pbl.nl/sites/default/files/downloads/pbl-2016-trends-in-global-co2-emisions-2016-report-2315_4.pdf.

[2] J. Lehne and F. Preston, "Making Concrete Change Innovation in Low-carbon Cement and Concrete The Royal Institute of International Affairs, Chatham House Report Series, www.chathamhouse.org/sites/default/files/publications/research/2018-06-13-makingconcrete- c," p. 138, 2018, [Online]. Available: www.chathamhouse.org.

[3] Bureau voor Normalisatie, "Geregistreerde Belgische norm norme belge enregistrée," no. september, p. 149, 2011.

[4] H. Beushausen, M. Alexander, and Y. Ballim, "Early-age properties, strength development and heat of hydration of concrete containing various South African slags at different replacement ratios," *Constr. Build. Mater.*, vol. 29, pp. 533–540, 2012, doi: 10.1016/j.conbuildmat.2011.06.018.

[5] S. Alahrache, F. Winnefeld, J. B. Champenois, F. Hesselbarth, and B. Lothenbach, "Chemical activation of hybrid binders based on siliceous fly ash and Portland cement," *Cem. Concr. Compos.*, vol. 66, pp. 10–23, 2016, doi: 10.1016/j.cemconcomp.2015.11.003.

[6] I. Wilińska, B. Pacewska, and A. Ostrowski, "Investigation of different ways of activation of fly ash–cement mixtures: Part 1. Chemical activation by Na2SO4 and Ca(OH)2," *J. Therm. Anal. Calorim.*, vol. 138, no. 6, pp. 4203–4213, 2019, doi: 10.1007/s10973-019-08485-1.

[7] S. Donatello, A. Fernández-Jimenez, and A. Palomo, "Very high volume fly ash cements. Early age hydration study using Na 2SO4 as an activator," *J. Am. Ceram. Soc.*, vol. 96, no. 3, pp. 900–906, 2013, doi: 10.1111/jace.12178.

[8] D. F. Velandia, C. J. Lynsdale, J. L. Provis, F. Ramirez, and A. C. Gomez, "Evaluation of activated high volume fly ash systems using Na2SO4, lime and quicklime in mortars with high loss on ignition fly ashes," *Constr. Build. Mater.*, vol. 128, pp. 248–255, 2016, doi: 10.1016/j.conbuildmat.2016.10.076.

[9] J. L. Provis, "Alkali-activated materials," *Cem. Concr. Res.*, vol. 114, pp. 40–48, 2018, doi: 10.1016/j.cemconres.2017.02.009.

[10] K. L. Scrivener, V. M. John, and E. M. Gartner, "Eco-efficient cements: Potential economically viable solutions for a low-CO2 cement-based materials industry," *Cem. Concr. Res.*, vol. 114, 2018, doi: 10.1016/j.cemconres.2018.03.015.

[11] X. Dai, S. Aydın, M. Y. Yardımcı, K. Lesage, and G. De Schutter, "Effect of Ca(OH)2 Addition on the Engineering Properties of Sodium Sulfate Activated Slag," *Materials (Basel).*, vol. 14, no. 15, p. 4266,

2021, doi: 10.3390/ma14154266.

[12] J. L. Provis, “Geopolymers and other alkali activated materials: Why, how, and what?,” *Mater. Struct. Constr.*, vol. 47, no. 1–2, pp. 11–25, 2014, doi: 10.1617/s11527-013-0211-5.

[13] J. L. Provis and J. S. J. van Deventer, *Alkali Activated Materials -State-of-the-Art Report, RILEM TC 224-AAM*, 1st ed. Springer, Dordrecht, 2013.

[14] S. A. Bernal, J. L. Provis, D. G. Brice, A. Kilcullen, P. Duxson, and J. S. J. Van Deventer, “Cement and Concrete Research Accelerated carbonation testing of alkali-activated binders signi fi cantly underestimates service life : The role of pore solution chemistry,” *Cem. Concr. Res.*, vol. 42, no. 10, pp. 1317–1326, 2012, doi: 10.1016/j.cemconres.2012.07.002.

[15] J. Fu *et al.*, “Mechanisms of enhancement in early hydration by sodium sulfate in a slag-cement blend – Insights from pore solution chemistry,” *Cem. Concr. Res.*, vol. 135, no. November 2019, 2020, doi: 10.1016/j.cemconres.2020.106110.

[16] E. Acevedo-Martinez, L. Y. Gomez-Zamorano, and J. I. Escalante-Garcia, “Portland cement-blast furnace slag mortars activated using waterglass: - Part 1: Effect of slag replacement and alkali concentration,” *Constr. Build. Mater.*, vol. 37, pp. 462–469, 2012, doi: 10.1016/j.conbuildmat.2012.07.041.

[17] B. Mota, T. Matschei, and K. Scrivener, “Impact of NaOH and Na2SO4 on the kinetics and microstructural development of white cement hydration,” *Cem. Concr. Res.*, vol. 108, no. February, pp. 172–185, 2018, doi: 10.1016/j.cemconres.2018.03.017.

[18] B. Mota, T. Matschei, and K. Scrivener, “The influence of sodium salts and gypsum on alite hydration,” *Cem. Concr. Res.*, vol. 75, pp. 53–65, 2015, doi: 10.1016/j.cemconres.2015.04.015.

[19] D. E. Angulo-Ramírez, W. G. Valencia-Saavedra, and R. M. de Gutiérrez, “Alkali-activated concretes based on fly ash and blast furnace slag: Compressive strength, water absorption and chloride permeability,” *Ing. e Investig.*, vol. 40, no. 2, pp. 72–80, 2020, doi: 10.15446/ing.investig.v40n2.83893.

[20] M. J. Sánchez-Herrero, A. Fernández-Jiménez, and A. Palomo, “C3S and C2S hydration in the presence of Na2CO3 and Na2SO4,” *J. Am. Ceram. Soc.*, vol. 100, no. 7, pp. 3188–3198, Jul. 2017, doi: https://doi.org/10.1111/jace.14855.

[21] B. Mota, T. Matschei, and K. Scrivener, “Impact of sodium gluconate on white cement-slag systems with Na2SO4,” *Cem. Concr. Res.*, vol. 122, no. August 2018, pp. 59–71, 2019, doi:

10.1016/j.cemconres.2019.04.008.

[22] F. Zunino and K. Scrivener, “Cement and Concrete Research Factors influencing the sulfate balance in pure phase C 3 S / C 3 A systems,” *Cem. Concr. Res.*, vol. 133, no. January, p. 106085, 2020, doi: 10.1016/j.cemconres.2020.106085.

[23] A. Adesina and C. Rodrigue, “Physico-mechanical and microstructural properties of sodium sulfate activated materials : A review,” *Constr. Build. Mater.*, vol. 295, p. 123668, 2021, doi: 10.1016/j.conbuildmat.2021.123668.

[24] H. Tan *et al.*, “Compressive strength and hydration process of wet-grinded granulated blast-furnace slag activated by sodium sulfate and sodium carbonate,” *Cem. Concr. Compos.*, vol. 97, no. January, pp. 387–398, 2019, doi: 10.1016/j.cemconcomp.2019.01.012.

[25] A. M. Rashad, “Influence of different additives on the properties of sodium sulfate activated slag,” *Constr. Build. Mater.*, vol. 79, pp. 379–389, 2015, doi: 10.1016/j.conbuildmat.2015.01.022.

[26] S. Uppalapati, L. Vandewalle, and Ö. Cizer, “Autogenous shrinkage of slag-fly ash blends activated with hybrid sodium silicate and sodium sulfate at different curing temperatures,” *Constr. Build. Mater.*, vol. 265, p. 121276, 2020, doi: 10.1016/j.conbuildmat.2020.121276.

[27] H. Nguyen, T. Chang, and A. Thymotie, “Enhancement of early engineering characteristics of modified slag cement paste with alkali silicate and sulfate,” *Constr. Build. Mater.*, vol. 230, p. 117013, 2020, doi: 10.1016/j.conbuildmat.2019.117013.

[28] A. M. Rashad, Y. Bai, P. A. M. Basheer, N. C. Collier, and N. B. Milestone, “Cement and Concrete Research Chemical and mechanical stability of sodium sulfate activated slag after exposure to elevated temperature,” *Cem. Concr. Res.*, vol. 42, no. 2, pp. 333–343, 2012, doi: 10.1016/j.cemconres.2011.10.007.

[29] A. M. Rashad, “An exploratory study on sodium sulfate activated slag modified with Portland cement,” *Mater. Struct. Constr.*, vol. 48, no. 12, pp. 4085–4095, 2015, doi: 10.1617/s11527-014-0468-3.

[30] S. D. Wang, K. L. Scrivener, and P. L. Pratt, “Factors affecting the strength of alkali-activated slag,” *Cem. Concr. Res.*, vol. 24, no. 6, pp. 1033–1043, 1994, doi: 10.1016/0008-8846(94)90026-4.

[31] I. Amer, M. Kohail, M. S. El-feky, A. Rashad, and M. A. Khalaf, “A review on alkali-activated slag concrete,” *Ain Shams Eng. J.*, vol. 12, no. 2, pp. 1475–1499, 2021, doi: 10.1016/j.asej.2020.12.003.

[32] S. A. Bernal *et al.*, “MgO content of slag controls phase evolution and structural changes induced by

accelerated carbonation in alkali-activated binders," *Cem. Concr. Res.*, vol. 57, pp. 33–43, 2014, doi: 10.1016/j.cemconres.2013.12.003.

[33] M. Ben Haha, B. Lothenbach, G. Le Saout, and F. Winnefeld, "Influence of slag chemistry on the hydration of alkali-activated blast-furnace slag - Part I: Effect of MgO," *Cem. Concr. Res.*, vol. 41, no. 9, pp. 955–963, 2011, doi: 10.1016/j.cemconres.2011.05.002.

[34] S. Joseph and Ö. Cizer, "Hydration of Hybrid Cements at Low Temperatures: A Study on Portland Cement-Blast Furnace Slag—Na2SO4," *Materials (Basel).*, vol. 15, no. 5, 2022, doi: 10.3390/ma15051914.

[35] W. Prince, M. Espagne, and P. Aı, "Ettringite formation : A crucial step in cement superplasticizer compatibility," vol. 33, pp. 635–641, 2003, doi: 10.1016/S0008-8846(02)01042-6.

[36] A. M. Rashad, Y. Bai, P. A. M. Basheer, N. B. Milestone, and N. C. Collier, "Hydration and properties of sodium sulfate activated slag," *Cem. Concr. Compos.*, vol. 37, no. 1, pp. 20–29, 2013, doi: 10.1016/j.cemconcomp.2012.12.010.

[37] L. Xue, Z. Zhang, and H. Wang, "Hydration mechanisms and durability of hybrid alkaline cements (HACs): A review," *Constr. Build. Mater.*, vol. 266, p. 121039, 2021, doi: 10.1016/j.conbuildmat.2020.121039.

[38] H. W. Reinhardt and C. U. Grosse, "Continuous monitoring of setting and hardening of mortar and concrete," *Constr. Build. Mater.*, vol. 18, no. 3, pp. 145–154, 2004, doi: 10.1016/j.conbuildmat.2003.10.002.

[39] M. Krüger, R. Bregar, G. A. David, and J. Juhart, "Non-destructive evaluation of eco-friendly cementituous materials by ultrasound," *Proc. Int. RILEM Conf. Mater. Syst. Struct. Civ. Eng.*, no. August, pp. 503–512, 2016.

[40] J. H. Kurz, C. U. Grosse, and H. W. Reinhardt, "Strategies for reliable automatic onset time picking of acoustic emissions and of ultrasound signals in concrete," *Ultrasonics*, vol. 43, no. 7, pp. 538–546, 2005, doi: 10.1016/j.ultras.2004.12.005.

[41] S.-U. Stuttgart, "SmartPick User Manual," no. V1.73, August 2012, pp. 0–13, 2012, [Online]. Available: http://www.smartmote.de.

[42] Smartmote - Universität Stuttgart, "FreshCon Duo User Manual," no. V.4.00 September 2012, pp. 0–34,

2012, [Online]. Available: http://www.smartmote.de.

[43] R. Snellings *et al.*, "Report of TC 238-SCM: hydration stoppage methods for phase assemblage studies of blended cements—results of a round robin test," *Mater. Struct. Constr.*, vol. 51, no. 4, 2018, doi: 10.1617/s11527-018-1237-5.

[44] J. S. Lumley, R. S. Gollop, G. K. Moir, and H. F. W. Taylor, "Degrees of reaction of the slag in some blends with Portland cements," *Cem. Concr. Res.*, vol. 26, no. 1, pp. 139–151, 1996, doi: 10.1016/0008-8846(95)00190-5.

[45] Y. A. Villagrán-Zaccardi, A. Vollpracht, E. Gruyaert, and N. De Belie, "Recommendation of RILEM TC 238-SCM: determination of the degree of reaction of siliceous fly ash and slag in hydrated cement paste by the selective dissolution method," *Mater. Struct. Constr.*, vol. 51, no. 1, 2018, doi: 10.1617/s11527-017-1134-3.

[46] J. Carette and S. Staquet, "Monitoring the setting process of mortars by ultrasonic P and S-wave transmission velocity measurement," *Constr. Build. Mater.*, vol. 94, pp. 196–208, 2015, doi: 10.1016/j.conbuildmat.2015.06.054.

[47] N. Robeyst, "Monitoring setting and microstructure development in fresh concrete with the ultrasonic through-transmission method.," Ghent University, Belgium, 2009.

[48] C. M. Sayers and R. L. Grenfell, "Ultrasonic propagation through hydrating cements," *Ultrasonics*, vol. 31, no. 3, pp. 147–153, 1993, doi: 10.1016/0041-624X(93)90001-G.

[49] A. Boumiz, C. Vernet, and F. Cohen Tenoudji, "Mechanical properties of cement pastes and mortars at early ages," *Adv. Cem. Based Mater.*, vol. 3, no. 3–4, pp. 94–106, 1996, doi: 10.1016/1065-7355(95)00072-0.

[50] P. Kumar Mehta and P. J. M. Monteiro, *Concrete: Microstructure, properties and materials.*, Third edit. Department of Civil and Environmental Engineering University of California at Berkeley: McGraw-Hill, 2006.

[51] Mohit Gupta and Dr. Arabinda Sharma, "The Effect of Water to Cement Ratio on Early Age Properties of Cement Paste and Mortar by UPV," *Int. J. Eng. Res.*, vol. V5, no. 05, pp. 550–556, 2016, doi: 10.17577/ijertv5is050698.

[52] G. S. M. Dehadrai, "Identifying the fluid-to-solid transition in cementitious materials at early ages using

ultrasonic wave velocity and computer simulation," no. April 2018, 2009.

[53] G. Trtnik and M. Gams, "The use of frequency spectrum of ultrasonic P-waves to monitor the setting process of cement pastes," *Cem. Concr. Res.*, vol. 43, no. 1, pp. 1–11, 2013, doi: 10.1016/j.cemconres.2012.10.002.

[54] H. K. Lee, K. M. Lee, Y. H. Kim, H. Yim, and D. B. Bae, "Ultrasonic in-situ monitoring of setting process of high-performance concrete," vol. 34, pp. 631–640, 2004, doi: 10.1016/j.cemconres.2003.10.012.

[55] K. L. Scrivener *et al.*, "TC 238-SCM: hydration and microstructure of concrete with SCMs: State of the art on methods to determine degree of reaction of SCMs," *Mater. Struct. Constr.*, vol. 48, no. 4, pp. 835–862, 2015, doi: 10.1617/s11527-015-0527-4.

[56] T. Kamada, S. Uchida, and K. Rokugo, "Nondestructive Evaluation of Setting and Hardening of Cement Paste Based on Ultrasonic Propagation Characteristics," 2005.

[57] F. Winnefeld and L. Holzer, "The ettringite – superplasticizer interaction and its impact on the ettringite distribution in cement suspensions," 2009.

[58] C. Jakob *et al.*, "Relating ettringite formation and rheological changes during the initial cement hydration: A comparative study applying XRD analysis, rheological measurements and modeling," *Materials (Basel).*, vol. 12, no. 18, 2019, doi: 10.3390/ma12182957.

[59] M. Wu *et al.*, "The influence of chemical admixtures on the strength and hydration behavior of lime-based composite cementitious materials," *Cem. Concr. Compos.*, vol. 103, no. May, pp. 353–364, 2019, doi: 10.1016/j.cemconcomp.2019.05.008.

[60] F. Zunino and K. Scrivener, "Insights on the role of alumina content and the filler effect on the sulfate requirement of PC and blended cements," *Cem. Concr. Res.*, vol. 160, no. July, p. 106929, 2022, doi: 10.1016/j.cemconres.2022.106929.

[61] N. De Belie, M. Soutsos, and E. Gruyaert, *Properties of Fresh and Hardened Concrete Containing Supplementary Cementitious Materials: State-of-the-Art Report of the RILEM Technical Committee 238-SCM, Working Group 4*. 2018.

[62] V. Kocaba, "Development and evaluation of methods to follow microstructural development of cementitious systems including slags," *Techniques*, vol. 4523, pp. 1–263, 2009, [Online]. Available: http://biblion.epfl.ch/EPFL/theses/2009/4523/4523_abs.pdf.

[63] D. B. N. Alderete, Natalia M., Villagran-Zaccardi Yury A., "Pore Refinement Action of GGBFS and Fly Ash on the Primery and Secondary Capillary Imbition Rates of Concrete," in *XV International conference on Durability of Building Materials and Components*, 2020, doi: 10.23967/dbmc.2020.192.

[64] Y. Villagrán-zaccardi, N. Alderete, P. Van den Heede, and N. De Belie, "Pore size distribution and surface multifractal dimension by multicycle mercury intrusion porosimetry of ggbfs and limestone powder blended concrete," *Appl. Sci.*, vol. 11, no. 11, 2021, doi: 10.3390/app11114851.

Appendix A. Supplementary data:

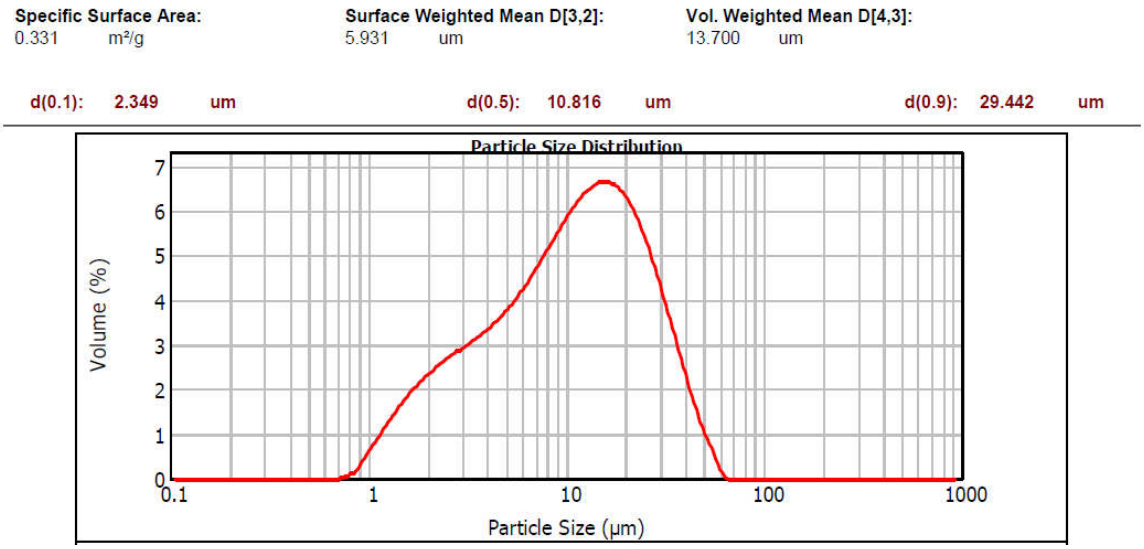

Figure A.1. Particle size distribution CEM I determined by laser diffraction.

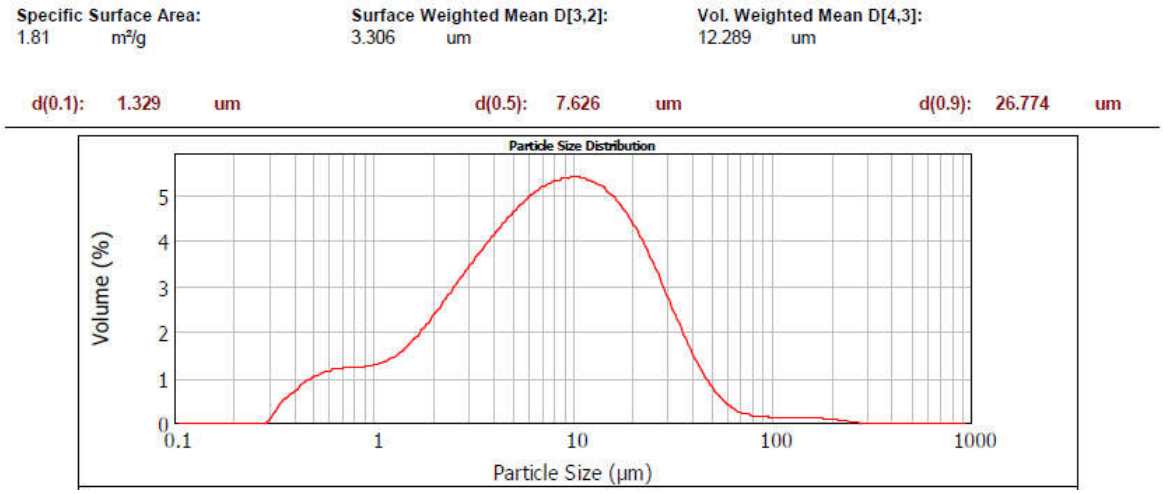

Figure A.2. Particle size distribution GGBFS determined by laser diffraction.

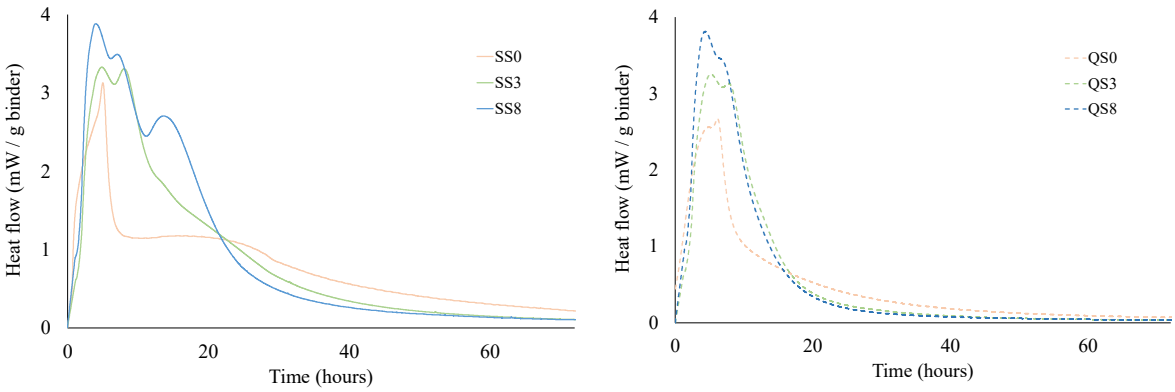

Figure A.3. Isothermal calorimetry at 37 ° C recorded for 7 days on pastes containing 0, 3 and 8% of sodium sulfate. Samples identified as SS contains GGBFS and PC while those identified as QS contain Quartz and PC.

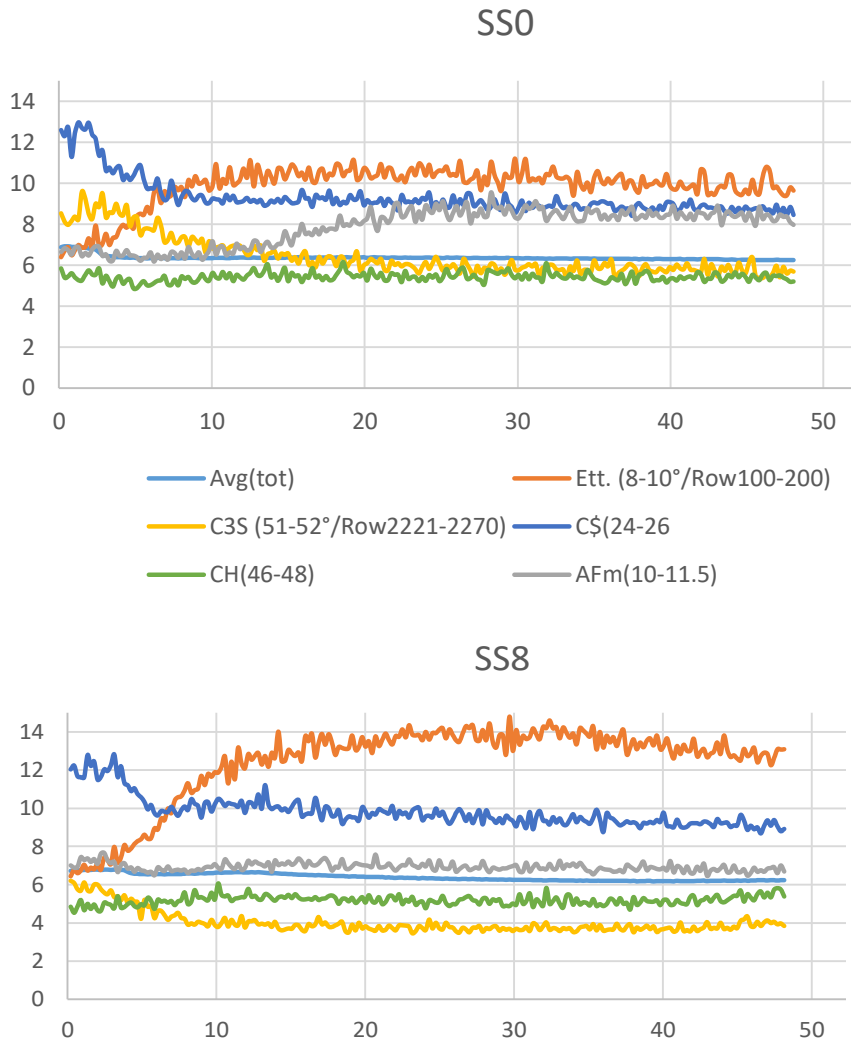

Figure A.4. Intensities from In-situ XRD at 37 º C recorded for 48 hours on pastes containing 0% (SS0) or 8% (SS8) of sodium sulfate. The information here is similar to the one plotted in Fig. 8 and 9 but in a different format.

Life cycle inventories (LCI) for SimaPro using data from the ecoinvent database:

Table A.1. Life cycle inventory, as implemented in SimaPro, for GGBFS when accounting for its basic treatment after production only (granulation + dewatering + drying + grinding + stock).

Outputs to technosphere	**Quantity**	**Unit**
GGBFS *(basic treatment (NL), T)*	1	kg
Known inputs from nature	**Quantity**	**Unit**

Water, unspecified natural origin, NL	0.01	m³
Known inputs from technosphere	**Quantity**	**Unit**
Electricity, medium voltage {NL} | market for | Cut-off, U *(granulation + dewatering)*	2.15×10^{-3}	kWh
Electricity, medium voltage {NL} | market for | Cut-off, U *(drying + grinding + stock)*	0.07	kWh
Natural gas, high pressure {NL} | market for | Cut-off, U *(drying + grinding + stock)*	8.25×10^{-3}	m³
Diesel {Europe without Switzerland} | market for | Cut-off, U *(drying + grinding + stock)*	9.49×10^{-4}	kg
Transport, freight train {Europe without Switzerland} | market for | Cut-off, U *(granulation + dewatering)*	3.00×10^{-3}	tkm
Transport, freight lorry > 32 metric ton {RER} | market for transport, freight lorry, lorry > 32 metric ton, EURO6 | Cut-off, U *(drying + grinding + stock)*	5.00×10^{-3}	tkm
Emissions to air	**Quantity**	**Unit**
Particulates *(granulation + dewatering)*	8.32×10^{-6}	kg
Particulates *(drying + grinding + stock)*	1.29×10^{-4}	kg
Sulfur oxides (*granulation + dewatering)*	2.07×10^{-4}	kg
Sulfur oxides *(drying + grinding + stock)*	6.84×10^{-7}	kg
Methane *(drying + grinding + stock)*	1.20×10^{-6}	kg
Nitrogen oxides *(drying + grinding + stock)*	2.17×10^{-5}	kg
Hydrogen sulfide *(drying + grinding + stock)*	2.43×10^{-4}	kg
Carbon monoxide *(granulation + dewatering)*	3.54×10^{-5}	kg
Carbon monoxide *(drying + grinding + stock)*	1.36×10^{-5}	kg
Outputs to technosphere: Waste treatment and emissions	**Quantity**	**Unit**
Sludge, pig iron production {Europe without Switzerland} | market for sludge, pig iron production | Cut-off, U	0.0015	kg

Waste water for pig iron production {Europe without Switzerland}| market for wastewater from pig iron production | Cut-off, U	0.003	m³

Table A.2. Life cycle inventory for GGBFS, as implemented in SimaPro, for GGBFS involving an economic allocation (E) of 0.84% cf. Chen et al. (2019) and no basic treatment (granulation + dewatering + drying + grinding + stock).

Outputs to technosphere	**Quantity**	**Unit**
Pig iron production ***(allocation %: 99.16 %)***	1	kg
GGBFS *(economic allocation (NL), cf. Chen et al. (2019), E)* ***(allocation %: 0.84%)***	0.24	kg
Known inputs from technosphere	**Quantity**	**Unit**
Pig iron {RoW} | pig iron production | Cut-off, U	1	kg

Table A.3. Life cycle inventory for GGBFS, as implemented in SimaPro, for GGBFS involving both basic treatment (granulation + dewatering + drying + grinding + stock, T) and an economic allocation (E) of 0.84% cf. Chen et al. (2019).

Outputs to technosphere	**Quantity**	**Unit**
GGBFS *(basic treatment + economic allocation, T+E)*	1	kg
Known inputs from technosphere	**Quantity**	**Unit**
GGBFS *(basic treatment (NL), T)*	1	kg
GGBFS *(economic allocation (NL), cf. Chen et al. (2019), E)* ***(allocation %: 0.84%)***	1	kg

Table A.4. Life cycle inventory, as implemented in SimaPro, for concrete mixing.

Outputs to technosphere	**Quantity**	**Unit**
Concrete mixing	1	m³
Known inputs from technosphere	**Quantity**	**Unit**
Concrete mixing factory {CH} | construction | Cut-off, U	4.17×10^{-7}	p

Lubricating oil {RER} | market for lubricating oil | Cut-off, U	0.02	kg
Synthetic rubber {GLO}| market for | Cut-off, U	0.12	kg
Diesel burned in building machine {GLO} | market for | Cut-off, U	0.2	MJ
Electricity, medium voltage {CH} | market for | Cut-off, U	5.4	kWh
Heat, district or industrial, natural gas {CH} | market for heat, district or industrial, natural gas | Cut-off, U	2.6	MJ
Heat, district or industrial, other than natural gas{CH} | heat production, light fuel oil, at industrial furnace 1 MW | Cut-off, U	2.4	MJ
Outputs to technosphere: Waste treatment and emissions	**Quantity**	**Unit**
Municipal solid waste {CH}| market for | Cut-off, U	0.05	kg
Waste concrete CH}| market for waste concrete | Cut-off, U	5.29	kg

Table A.5. Life cycle inventory, as implemented in SimaPro, for mortar mix SS0 considering only basic treatment (T) for the GGBFS.

Outputs to technosphere	**Quantity**	**Unit**
SS0 *(basic treatment, T)*	2319.29	kg
Known inputs from technosphere	**Quantity**	**Unit**
Cement, Portland {Europe without Switzerland} | production|Cut-off, U	156.36	kg
Tap water {Europe without Switzerland} | market for|Cut-off, U	234.53	kg
Sand {CH} | market for sand | Cut-off, U	1563.56	kg
GGBFS *(basic treatment (NL), T)*	364.83	kg
Sodium sulfate, anhydrite {RoW} | market for | Cut-off, U	0.00	kg
Concrete mixing	1	m^3

Table A.6. Life cycle inventory, as implemented in SimaPro, for mortar mix SS0 considering basic treatment + economic allocation (T+E) for the GGBFS.

Outputs to technosphere	**Quantity**	**Unit**

SS0 *(basic treatment + economic allocation, T+E)*	2319.29	kg
Known inputs from technosphere	**Quantity**	**Unit**
Cement, Portland {Europe without Switzerland} | production | Cut-off, U	156.36	kg
Tap water {Europe without Switzerland} | market for | Cut-off, U	234.53	kg
Sand {CH} | market for sand | Cut-off, U	1563.56	kg
GGBFS *(basic treatment + economic allocation, T+E)*	364.83	kg
Sodium sulfate, anhydrite {RoW} | market for | Cut-off, U	0.00	kg
Concrete mixing	1	m^3

Table A.7. Life cycle inventory, as implemented in SimaPro, for mortar mix SS3 considering only basic treatment (T) for the GGBFS.

Outputs to technosphere	**Quantity**	**Unit**
SS3 *(basic treatment, T)*	2320.82	kg
Known inputs from technosphere	**Quantity**	**Unit**
Cement, Portland {Europe without Switzerland} | production | Cut-off, U	155.73	kg
Tap water {Europe without Switzerland} | market for | Cut-off, U	233.59	kg
Sand {CH} | market for sand | Cut-off, U	1557.25	kg
GGBFS *(basic treatment (NL), T)*	363.36	kg
Sodium sulfate, anhydrite {RoW} | market for | Cut-off, U	10.90	kg
Concrete mixing	1	m^3

Table A.8. Life cycle inventory, as implemented in SimaPro, for mortar mix SS3 considering basic treatment + economic allocation (T+E) for the GGBFS.

Outputs to technosphere	**Quantity**	**Unit**
SS3 *(basic treatment + economic allocation, T+E)*)	2320.82	kg
Known inputs from technosphere	**Quantity**	**Unit**
Cement, Portland {Europe without Switzerland} | production | Cut-off, U	155.73	kg

Tap water {Europe without Switzerland} | market for | Cut-off, U	233.59	kg
Sand {CH} | market for sand | Cut-off, U	1557.25	kg
GGBFS *(basic treatment + economic allocation, T+E)*	363.36	kg
Sodium sulfate, anhydrite {RoW} | market for | Cut-off, U	10.90	kg
Concrete mixing	1	m^3

Table A.9. Life cycle inventory, as implemented in SimaPro, for mortar mix SS5 considering only basic treatment (T) for the GGBFS.

Outputs to technosphere	**Quantity**	**Unit**
SS5 *(basic treatment, T)*	2321.84	kg
Known inputs from technosphere	**Quantity**	**Unit**
Cement, Portland {Europe without Switzerland} | production | Cut-off, U	155.31	kg
Tap water {Europe without Switzerland} | market for | Cut-off, U	232.96	kg
Sand {CH} | market for sand | Cut-off, U	1553.07	kg
GGBFS *(basic treatment (NL), T)*	362.38	kg
Sodium sulfate, anhydrite {RoW} | market for | Cut-off, U	18.12	kg
Concrete mixing	1	m^3

Table A.10. Life cycle inventory, as implemented in SimaPro, for mortar mix SS5 considering basic treatment + economic allocation (T+E) for the GGBFS.

Outputs to technosphere	**Quantity**	**Unit**
SS5 *(basic treatment + economic allocation, T+E)*	2321.84	kg
Known inputs from technosphere	**Quantity**	**Unit**
Cement, Portland {Europe without Switzerland} | production | Cut-off, U	155.31	kg
Tap water {Europe without Switzerland} | market for | Cut-off, U	232.96	kg
Sand {CH} | market for sand | Cut-off, U	1553.07	kg
GGBFS *(basic treatment + economic allocation, T+E)*	362.38	kg

Sodium sulfate, anhydrite {RoW} | market for | Cut-off, U	18.12	kg
Concrete mixing	1	m³

Table A.11. Life cycle inventory, as implemented in SimaPro, for mortar mix SS8 considering only basic treatment (T) for the GGBFS.

Outputs to technosphere	**Quantity**	**Unit**
SS8 *(basic treatment, T)*	2323.36	kg
Known inputs from technosphere	**Quantity**	**Unit**
Cement, Portland {Europe without Switzerland} | production | Cut-off, U	154.68	kg
Tap water {Europe without Switzerland} | market for | Cut-off, U	232.03	kg
Sand {CH} | market for sand | Cut-off, U	1546.84	kg
GGBFS *(basic treatment (NL), T)*	360.93	kg
Sodium sulfate, anhydrite {RoW} | market for | Cut-off, U	28.87	kg
Concrete mixing	1	m³

Table A.12. Life cycle inventory, as implemented in SimaPro, for mortar mix SS8 considering basic treatment + economic allocation (T+E) for the GGBFS.

Outputs to technosphere	**Quantity**	**Unit**
SS8 *(basic treatment + economic allocation, T+E)*	2323.36	kg
Known inputs from technosphere	**Quantity**	**Unit**
Cement, Portland {Europe without Switzerland} | production | Cut-off, U	154.68	kg
Tap water {Europe without Switzerland} | market for | Cut-off, U	232.03	kg
Sand {CH} | market for sand | Cut-off, U	1546.84	kg
GGBFS *(basic treatment + economic allocation, T+E)*	360.93	kg
Sodium sulfate, anhydrite {RoW} | market for | Cut-off, U	28.87	kg
Concrete mixing	1	m³

Table A.13. Life cycle inventory, as implemented in SimaPro, for mortar mix SS10 considering only basic treatment (T) for the GGBFS.

Outputs to technosphere	**Quantity**	**Unit**
SS10 *(basic treatment, T)*	2324.36	kg
Known inputs from technosphere	**Quantity**	**Unit**
Cement, Portland {Europe without Switzerland} | production | Cut-off, U	154.27	kg
Tap water {Europe without Switzerland} |market for | Cut-off, U	231.41	kg
Sand {CH} | market for sand | Cut-off, U	1542.72	kg
GGBFS *(basic treatment (NL), T)*	359.97	kg
Sodium sulfate, anhydrite {RoW} |market for | Cut-off, U	36.00	kg
Concrete mixing	1	m^3

Table A.14. Life cycle inventory, as implemented in SimaPro, for mortar mix SS10 considering basic treatment + economic allocation (T+E) for the GGBFS.

Outputs to technosphere	**Quantity**	**Unit**
SS10 *(basic treatment + economic allocation, T+E)*	2324.36	kg
Known inputs from technosphere	**Quantity**	**Unit**
Cement, Portland {Europe without Switzerland} | production | Cut-off, U	154.27	kg
Tap water {Europe without Switzerland} | market for | Cut-off, U	231.41	kg
Sand {CH} | market for sand | Cut-off, U	1542.72	kg
GGBFS *(basic treatment + economic allocation, T+E)*	359.97	kg
Sodium sulfate, anhydrite {RoW} | market for | Cut-off, U	36.00	kg
Concrete mixing	1	m^3

Abbreviations

CH: Switzerland; E: Economic allocation; GGBFS: Ground Granulated Blast Furnace Slag; GLO: ecoinvent data for Global; LCI: Life Cycle Inventory; NL: the Netherlands; RER: ecoinvent data for Europe as geographical

region; RoW: ecoinvent data for Rest-of-the-World as geographical region; T: basic treatment; U: ecoinvent unit process.

References

Chen, X.; Wang, H.; Najm, H.; Venkiteela, G.; Hencken, J. Evaluating engineering properties and environmental impact of pervious concrete with fly ash and slag. J. Clean. Prod. 2019, 237, 11.